Metabolism Clinical and Experimental 116 (2021) 154463

Contents lists available at ScienceDirect

Metabolism Clinical and Experimental

journal homepage: www.metabolismjournal.com

Inhibiting glycolysis rescues memory impairment in an intellectual disability *Gdi1*-null mouse

Patrizia D'Adamo [a,b,c,*], Anemari Horvat [b,c], Antonia Gurgone [a,1], Maria Lidia Mignogna [a], Veronica Bianchi [a,2], Michela Masetti [a,3], Maddalena Ripamonti [a], Stefano Taverna [a], Jelena Velebit [b,c], Maja Malnar [b], Marko Muhič [b], Katja Fink [b], Angela Bachi [d], Umberto Restuccia [d,4], Sara Belloli [e,f], Rosa Maria Moresco [f,g], Alessia Mercalli [h], Lorenzo Piemonti [h,i], Maja Potokar [b,c], Saša Trkov Bobnar [b,c], Marko Kreft [b,c,j], Helena H. Chowdhury [b,c], Matjaž Stenovec [b,c], Nina Vardjan [b,c,**], Robert Zorec [b,c,**]

[a] *Division of Neuroscience, IRCCS San Raffaele Scientific Institute, Milan, Italy*
[b] *University of Ljubljana, Faculty of Medicine, Institute of Pathophysiology, Laboratory of Neuroendocrinology – Molecular Cell Physiology, Ljubljana, Slovenia*
[c] *Celica Biomedical, Laboratory for Cell Engineering, Ljubljana, Slovenia*
[d] *IFOM, the FIRC Institute of Molecular Oncology, Milan, Italy*
[e] *Institute of Bioimaging and Physiology, CNR, Segrate (MI), Italy*
[f] *Experimental Imaging Center (EIC), San Raffaele Scientific Institute, Milan, Italy*
[g] *Medicine and Surgery Department, University of Milano-Bicocca, Monza (MB), Italy*
[h] *Diabetes Research Institute, IRCCS Ospedale San Raffaele, Milano, Italy*
[i] *Università Vita-Salute San Raffaele, Milano, Italy*
[j] *University of Ljubljana, Biotechnical Faculty, Department of Biology, Ljubljana, Slovenia*

ARTICLE INFO

Article history:
Received 18 September 2020
Accepted 4 December 2020

Keywords:
Aerobic glycolysis
Intellectual disability
Astrocytes
cAMP
GDI1 knockout mice

ABSTRACT

Objectives: *GDI1* gene encodes for αGDI, a protein controlling the cycling of small GTPases, reputed to orchestrate vesicle trafficking. Mutations in human *GDI1* are responsible for intellectual disability (ID). In mice with ablated *Gdi1*, a model of ID, impaired working and associative short-term memory was recorded. This cognitive phenotype worsens if the deletion of αGDI expression is restricted to neurons. However, whether astrocytes, key homeostasis providing neuroglial cells, supporting neurons via aerobic glycolysis, contribute to this cognitive impairment is unclear.

Methods: We carried out proteomic analysis and monitored [^{18}F]-fluoro-2-deoxy-D-glucose uptake into brain slices of *Gdi1* knockout and wild type control mice. D-Glucose utilization at single astrocyte level was measured by the Förster Resonance Energy Transfer (FRET)-based measurements of cytosolic cyclic AMP, D-glucose and L-lactate, evoked by agonists selective for noradrenaline and L-lactate receptors. To test the role of astrocyte-resident processes in disease phenotype, we generated an inducible *Gdi1* knockout mouse carrying the *Gdi1* deletion only in adult astrocytes and conducted behavioural tests.

Results: Proteomic analysis revealed significant changes in astrocyte-resident glycolytic enzymes. Imaging [^{18}F]-fluoro-2-deoxy-D-glucose revealed an increased D-glucose uptake in *Gdi1* knockout tissue versus wild type control mice, consistent with the facilitated D-glucose uptake determined by FRET measurements. In mice with *Gdi1* deletion restricted to astrocytes, a selective and significant impairment in working memory was recorded, which was rescued by inhibiting glycolysis by 2-deoxy-D-glucose injection.

Abbreviations: cAMP, cyclic adenosine monophosphate; CNS, central nervous system; CFP, cyan fluorescent protein; CS, conditional stimulus, tone; CTX, context memory; [^{18}F]-FDG, [^{18}F]-fluoro-2-deoxy-D-glucose; FRET, Förster Resonance Energy Transfer; *GDI1*, guanosine dissociation inhibitor 1 gene; *GlastGdi1flox/Y*, *GLAST:CreERT2 +/Gdi1lox/Y* inducible astrocyte-specific *Gdi1* KO male mice; *GlastGdi1X/Y*, male mice (*Gdi1X/Y*) carrying the *GLAST:CreERT2* transgene; *Gdi1* KO, full knockout of *Gdi1*; *Gdi1* WT, wild type; αGDI, α guanosine dissociation inhibitor protein coded by *GDI1* gene; GFAP, glial fibrillary acidic protein; GLUT1, D-glucose transporter; 2-DG, 2-deoxy-D-glucose; GPR81, G-protein receptor 81; GPCR, G-protein coupled receptor; MCTs, monocarboxylate transporters; NA, noradrenaline; 3-Cl-5-OH-BA, 3-chloro-5-hydroxybenzoic acid; PKA, protein kinase A; PSD, postsynaptic density; SEM, standard error of the mean; sEPSCs, spontaneous excitatory postsynaptic currents; SV, synaptic vesicle; XLID, X-linked intellectual disability; YFP, yellow fluorescent protein.

* Correspondence to: P. D'Adamo, Division of Neuroscience, IRCCS San Raffaele Scientific Institute, Milan, Italy.
** Corresponding authors at: University of Ljubljana, Faculty of Medicine, Institute of Pathophysiology, Laboratory of Neuroendocrinology – Molecular Cell Physiology, Ljubljana, Slovenia.
E-mail addresses: dadamo.patrizia@hsr.it (P. D'Adamo), nina.vardjan@mf.uni-lj.si (N. Vardjan), robert.zorec@mf.uni-lj.si (R. Zorec).
[1] Present address: Department of Neuroscience "Rita Levi Montalcini", University of Turin, Turin, Italy.
[2] Present address: no current professional address.
[3] Present address: Humanitas Clinical and Research Center - IRCCS, Rozzano, Italy.
[4] Present address: Adienne Srl SU, Caponago, Italy.

https://doi.org/10.1016/j.metabol.2020.154463

Conclusions: These results reveal a new astrocyte-based mechanism in neurodevelopmental disorders and open a novel therapeutic opportunity of targeting aerobic glycolysis, advocating a change in clinical practice.

1. Introduction

Human intellectual disability is a common human neurodevelopmental disorder with an early onset in postnatal life, affecting approximately 1%–3% of the population [1]. In recent years, >100 different X-linked genes encoding for proteins with a large variety of functions have been identified [2–4]. Thus, the final phenotypic outcome of intellectual disability appears to reflect many different types of abnormal cellular processes leading to neuronal dysfunction [2].

Mutations in the human *GDI1* gene cause X-linked intellectual disability (XLID) clinically characterized by "pure" cognitive deficit without additional clinical features [5]. This gene encodes for αGDI, a protein that controls the cycling of RAB GTPases, which in turn orchestrate specific vesicular trafficking steps by switching from an active GTP-bound conformation to an inactive GDP-bound conformation [6]. The role of αGDI is to actively retrieve GDP-bound RAB GTPases from the membrane to form a soluble cytosolic complex of inactive RAB proteins.

In line with this, it has been demonstrated that full ablation of *Gdi1* (*Gdi1* knockout [KO]) impaired hippocampal-dependent forms of short-term memory; namely, working and associative fear-related memory formation [7]. This cognitive deficit has also been observed in a conditional *Gdi1* KO (*CaMKII-Cre*$^{+}$*-Gdi1*$^{flox/Y}$) murine model, where gene inactivation occurred solely in post-mitotic neurons of the adult anterior forebrain. Moreover, electrophysiological comparison at cortico-amygdala synaptic connections between the *Gdi1* KO and conditional *Gdi1* mice revealed a stronger pre-synaptic phenotype in conditional *Gdi1* mice, confirming the pivotal role of αGDI in hippocampal, cortical and amygdala synapses in the process of memory formation [8]. Although XLID-related cellular defects arise from impaired neuronal processes, it is also possible that altered function of astrocytes contributes to the behavioural phenotype in *Gdi1* KO animals, as astroglia are the key cell type providing homeostasis and represent a central element in neuropathology [9,10].

Here, we investigated whether astrocytes, bearing important pathological potential, contribute to the phenotype of XLID [10,11]. The results reveal that by limiting *Gdi1* deletion to astrocytes in an inducible conditional *Gdi1* KO mouse (*GlastGdi1*$^{flox/Y}$), the behavioural deficit is restricted to alteration in working memory. This cognitive deficit is associated with impaired astrocytic aerobic glycolysis, characterized by facilitated D-glucose utilization controlled by receptor-mediated cAMP signalling. Moreover, inhibition of glycolysis by the injection of 2-deoxy-D-glucose (2-DG) [12] improves the *Gdi1* KO mice behavioural phenotype, revealing a new astrocyte-based therapeutic targeting opportunity for this form of XLID.

2. Methods and materials

Unless noted otherwise, all chemicals were of the highest quality available and purchased from Sigma-Aldrich (Merck KGaA, Darmstadt, Germany).

2.1. Cell culture and transfection

Primary astrocytes were isolated from cortices of P2 *Gdi1* WT and *Gdi1* KO mice as described [13] and grown as in Giannandrea et al. [14]. Transfection with plasmids carrying FRET-based nanosensors was performed with FuGENE 6 transfection reagent according to the manufacturer's instructions (Promega, Madison, WI, USA).

The experimental protocol was approved by The Administration of the Republic of Slovenia for Food Safety, Veterinary and Plant Protection (Republic of Slovenia, Ministry of Agriculture, Forestry and Food, Dunajska cesta 22, 1000 Ljubljana), Document No. U34401-47/2014/7, signed by Barbara Tomše, DVM.

2.2. SILAC proteomics

Primary astrocytic cells were labelled by culturing them for 14 days in the appropriate medium containing the light (for *Gdi1* WT labelling: L) and heavy (for *Gdi1* KO labelling: H) versions of arginine and lysine. Once complete incorporation had occurred, cells were harvested, counted and mixed 1:1 (<3 million of cells per sample) and the subcellular compartments (cytosol, membrane, nucleus and cytoskeleton) were fractionated using a Qproteome Cell Compartment kit (QIAGEN, Dusseldorf, Germany), following the manufacturer's instructions. Samples were precipitated with acetone to get rid of salts and contaminants, re-suspended in RIPA buffer (500 mM Tris-HCl [pH 7.4], 200 mM NaCl, 1 mM EDTA, 1% Triton X-100, 1% NP-40, protease inhibitor cocktail), and then proteins were resolved on a pre-cast SDS-PAGE gel, 4%–12% (Invitrogen, Carlsbad, CA, USA) and stained using colloidal Coomassie (Bio-Rad, Hercules, CA, USA). Single lanes were then cut into bands, each band was chopped into small pieces, reduced with 1,4-dithiothreitol (DTT), alkylated with iodoacetamide, digested with trypsin [15] and desalted using StageTip (Proxeon Biosystems, Odense, Denmark). Resulting peptides were resolved onto a 15-cm-long C18 column. A 95-min long gradient of eluents A (pure water with 2% v/v acetonitrile [ACN], 0.5% v/v acetic acid) and B (ACN with 2% v/v pure water with 0.5% v/v acetic acid) was used to achieve separation, from 7% B (at 0 min, 0.2 μL/min flow rate) to 70% B (at 95 min, 0.2 μL/min flow rate). The liquid chromatography system was connected to an LTQ Orbitrap mass spectrometer (Thermo Scientific, Bremen, Germany) equipped with a nanoelectrospray ion source (Proxeon Biosystems, Odense, Denmark). The acquisition mass range for each sample was from m/z 350 to 1700 Da, and the analyses were done in duplicate. Full scans were acquired at high resolution ($R = 60{,}000$ at 400 m/z), and the automatic gain control (AGC) target was set to 1×10^6 at a maximum injection time of 500 ms. The 15 most intense peaks were automatically selected, fragmented by collision-induced dissociation set at 37, and acquired in the linear ion trap at low resolution, AGC target 1×10^4, and 3 microscans of 150 ms each. Ions acquired twice were dynamically excluded for further selection and fragmentation for 90 s. Spectra were loaded into MaxQuant software (version 1.1.1.25) [16] and searched against the mouse International Protein Index database (release 20100819) using the Andromeda search engine [17]. Search parameters were as follows: trypsin strict specificity for cleavage, carbamidomethylation as fixed modification, methionine oxidation, and protein N-terminal acetylation as variable modifications, 2 missed cleavages allowed, 10 ppm tolerance for the precursor, and 0.5 Da tolerance for the fragment ions. To be considered as identified, proteins had to pass the following criteria: minimum peptide length of 6, at least 1 assigned peptide and 1 unique peptide. The false discovery rate for both peptides and proteins was set at 0.01. Keratins and proteins derived from foetal calf serum have been removed from further analysis. SILAC quantification was done according to the MaxQuant algorithm on razor and unique peptides, with at least 1 ratio count. Statistical analysis was performed using Perseus tools available in the MaxQuant environment.

2.3. [^{18}F]-fluoro-2-deoxy-D-glucose uptake

[^{18}F]-FDG was prepared for clinical use as indicated in the European Pharmacopeia, VIII edition. Autoradiography experiments were performed on 3-months-old mice sacrificed 1 h after tail vein injection of 135.3 ± 19.7 μCi [^{18}F]-FDG. Brain was rapidly removed and placed into a specific brain matrix (Stoelting, Wood Dale, IL, USA); 2-mm slices were cut with stainless steel blades and exposed for 1 h to a phosphor screen. After that, images were acquired with PhosphorImager (CycloneScan, Perkin Elmer, Waltham, MA, USA) and analysed using Optiquant software. [^{18}F] radioactivity in mouse brains was calculated as a percentage of the injected dose (ID) per brain area analysed (%ID/mm^2). Two types of analysis were performed using the region of interest (ROI): for the first, each slice was surrounded manually and contained radioactivity reported as the sum of all slices (% of total brain); for the second, different brain areas (cortex, striatum, hippocampus, thalamus and cerebellum) were surrounded manually to obtain %ID/mm^2.

2.4. Glucose measurements

Blood glucose was determined using the Roche ACCU−CHEK® Active meter. Serum levels of insulin and C-peptide were detected using multiplex bead-based assays based on x Multi-Analyte Profile technology (MILLIPLEX MAP Mouse Metabolic Hormone Magnetic Bead panel). Assay was performed following the manufacturer's protocols and run on MAGPIX (Biorad) with Bio-Plex manager software v6.1 (Bio-Rad). Oral glucose tolerance test (OGTT) was performed on mice that were fasted at least for 12 h. Animals were orally administered, by oral gavage, with glucose solution (1 mg/g BW). Blood glucose was determined from the tail vein at seven-time points: 0 (before glucose load), 10 (10 min after glucose load), 20, 30, 60, 90 and 120 min. Insulin tolerance test (ITT) was performed as follows: the mice were fasted for 4 h and intraperitoneally injected with 0,75 U/kg BW of insulin (Actrapid, Novo Nordisk). Blood glucose was determined from the tail vein at eight-time points: 0 (before insulin load), 15 (15 min after insulin load), 30, 45, 60, 75, 90 and 120 min.

2.5. Immunohistochemistry

Harvested tissues were fixed in 10% buffered formalin, embedded in paraffin, cut and stained with hematoxylin and eosin for morphological analysis. For immunohistochemical analysis, 3 μm sections were incubated with polyclonal anti-glucose transporter GLUT1 antibody (1:200; Abcam, Cambridge, UK, ab15309) or anti-GFAP (1:500; Dako, Glostrup, Denmark, Z0334) after antigen retrieval with Tris-EDTA (pH 9) in a warm bath, and the immunoreaction was revealed with a rabbit-on-rodent HRP-polymer (Biocare Medical, Pacheco, CA, USA), using 3,3-diaminobenzidine as chromogen and counterstaining with hematoxylin.

2.6. Immunostainings, in situ hybridization and image analysis

Immunofluorescence staining on primary cultured astrocytes was performed as described [7]. The following primary antibodies were used: rabbit polyclonal anti-MCT1 (1:50; Abcam, Cambridge, UK, ab93048), rabbit polyclonal anti-MCT4 (1:50; Santa Cruz Biotechnology, Dallas, TX, USA, SC-50329), rabbit monoclonal anti-α_{1A}-AR (1:1000; Abcam, Cambridge, UK, ab137123), rabbit polyclonal anti-α_{2A}-AR (1:100; Biorbyt, Cambridge, UK, orb10054), rabbit polyclonal anti β_1-AR (1:200; Abcam, Cambridge, UK, ab85037), rabbit polyclonal β_2-AR (1:100; Biorbyt, Cambridge, UK, orb10056) or rabbit polyclonal β_3-AR (1:100; Biorbyt, Cambridge, UK, orb10057). Images were acquired using an inverted Zeiss LSM510 META confocal microscope with an oil immersion plan apochromatic objective (63×, 1.4 NA; Carl Zeiss, Jena, Germany) and 488-nm Ar-ion laser excitation. Emission spectra were acquired with a 505–530-nm bandpass emission filter or >505 nm longpass emission filter. The number of MCT1-, MCT4-, α_{1A}-AR-, α_{2A}-AR-, β_1-AR-, β_2-AR- and β_3-AR-positive green fluorescence pixels above the intensity threshold set at 20% and the number of all pixels (total cell pixels) were determined in individual cells using the ROI tool in the LSM 510 META software. The percentage of positive pixels (green labelled) versus total cell pixel area was calculated in *Gdi1* WT and *Gdi1* KO astrocytes using Excel (Microsoft, Seattle, WA, USA). In the case of ARs, the values were normalized to mean values of WT astrocytes for each receptor separately.

Murine brain slices were prepared and immunostained as described by Bianchi et al. [8]. Monoclonal anti-GFAP antibody was used (1:100; Sigma-Aldrich, St. Louis, MO, USA, G-3893). When immunofluorescence was coupled to in situ hybridization, this was performed as in D'Adamo et al. [7]. Images were captured using a Zeiss AxioImager M2m (Carl Zeiss, Jena, Germany) equipped with a 10× objective. GFAP density was calculated using the Gran Filter plugin for ImageJ (NIH, Bethesda, MD, USA) and normalized on the area being considered. Colocalization between *Gdi1* and GFAP was analysed using the Colocalization plugin for ImageJ.

2.7. Surface biotinylation

Biotinylation assays on cultured primary astrocytes were performed as described in Diering et al. [18]. Then western blot (WB) experiments were performed by loading protein extracts onto a 12% polyacrylamide gel, then transferred to a nitrocellulose membrane using a TurboBlot machine (Bio-Rad). Polyclonal anti-GLUT1 (WB 1:500; Abcam, Cambridge, UK, ab15309), polyclonal anti-αGDI (WB 1:20,000; Invitrogen, Carlsbad, California, USA, 71-0300) antibodies were used, and polyclonal anti-Calnexin (WB 1:10,000; Sigma, St. Louis, Missouri, USA, C-4731) was employed to normalize the total amount of protein. Analyses were done using ImageJ software.

2.8. FRET measurements of cAMP-dependent PKA activity

Gdi1 WT and *Gdi1* KO astrocytes expressing the FRET-based PKA nanosensor AKAR2 [19] were examined 24–48 h after transfection with a Plan NeoFluar 40×/1.3 oil differential interference contrast immersion objective (Carl Zeiss) using a Zeiss LSM510 META confocal microscope (Carl Zeiss). Cells were excited at 458 nm, and images (512 × 512) were acquired every 3.5 s using lambda stack acquisition. Emission spectra were collected from the META detector in 8 channels (lambda stack) ranging from 470 nm to 545 nm, each 10.7 nm wide. Two-channel (cyan fluorescent protein [CFP] and yellow fluorescent protein [YFP]) images were generated using the analytical software Extract channels (Zeiss LSM510 META). Channels with emission spectra at 470 and 481 nm and emission spectra at 513, 524, and 534 nm were extracted to the CFP and YFP channels, respectively. YFP and CFP fluorescence intensities were quantified within an ROI selected for individual cells expressing AKAR2 using the LSM510 META software. In the graphs, the FRET ratio signal was reported as the ratio of the YFP/CFP (AKAR2) fluorescence signals after subtracting the background fluorescence from the signals using Excel. The values of the FRET signals were normalized to 1.0. An increase in the FRET signal reflects an increase in cAMP-dependent PKA activity.

Initially, astrocytes were kept in an extracellular solution (10 mM HEPES/NaOH [pH 7.2], 10 mM D-glucose, 131.8 mM NaCl, 1.8 mM $CaCl_2$, 2 mM $MgCl_2$, 5 mM KCl, 0.5 mM $NaH_2PO_4 \cdot H_2O$, and 5 mM $NaHCO_3$) and were then treated with various reagents following a 100-s baseline: 100 μM NA, 2 or 20 mM L-lactate or 0.5 mM 3Cl-5OH-BA (Santa Cruz Biotechnology, Dallas, TX, USA). The osmolality of the extracellular solution was ~300 mOsm, measured with a freezing point osmometer (Osmomat 030, Gonotech, Berlin, Germany).

2.9. FRET measurements of $[glucose]_i$ and $[lactate]_i$

Gdi1 WT and *Gdi1* KO astrocytes expressing the FRET-based glucose nanosensor FLII12PGLU-700 μΔ6 (www.addgene.org) [20,21] or the FRET-based lactate nanosensor Laconic [22] were examined 16–48 h after transfection with a fluorescence microscope (Zeiss Axio Observer.AI, Zeiss, Oberkochen, Germany), with a CCD camera and monochromator Polychrome V (Till Photonics, Graefelfing, Germany) as a monochromatic source of light with a wavelength 436 nm/10 nm. Dual emission intensity ratios were recorded using an image splitter (Optical Insights, Tucson, AZ, USA) and 2 emission filters; 465/30 nm for ECFP or mTFP and 535/30 nm for EYFP or Venus. Images were acquired at 10 s with an exposure time of 0.1 s. The background fluorescence was subtracted from individual EYFP or Venus and ECFP or mTFP fluorescence signals. The FRET ratio signals, EYFP/ECFP (FLII12PGLU-700μΔ6) and mTFP/Venus (Laconic), were obtained from integration of the ratio signal over the entire cell using Life Acquisition software (Till Photonics, Graefelfing, Germany). The values of the FRET signals were normalized to 1.0. An increase in the FRET ratio signal reflects increases in the $[glucose]_i$ and $[lactate]_i$.

Initially, cells were kept in extracellular solution (10 mM HEPES/NaOH [pH 7.2], 3 mM D-glucose, 135.3 mM NaCl, 1.8 mM $CaCl_2$, 2 mM $MgCl_2$, 5 mM KCl, 0.5 mM $NaH_2PO_4 \cdot H_2O$, 5 mM $NaHCO_3$), after which they were treated with various reagents following a baseline: 200 μM NA, 20 mM L-lactate or 6 mM CHC (Sigma-Aldrich), an MCT blocker. In some of the experiments cells were pre-incubated in extracellular solution without D-glucose, with 3 mM 2-DG, and with a mixture of 1.5 mM D-glucose and 1.5 mM 2-DG for 30 min at 37 °C and then stimulated with 200 μM NA in the incubating solutions. The solution with CHC was prepared by diluting CHC ethanol stock solution (130 mM) in the extracellular solution. The final concentration of ethanol was 4.6%, which did not significantly influence the FRET signal.

Extracellular solution osmolality was ~300 mOsm/L, as measured with an Osmomat 030 osmometer.

2.10. FRET signal analysis

Single exponential and double exponential increases to maximum functions ($F = F_0 + c \times (1 - \exp(-t/\tau))$ or $F = F_0 + c_1 \times (1 - \exp(-t/\tau_1) + c_2 \times (1 - \exp(-t/\tau_2)))$, respectively) were fitted to the diagrams with FRET ratio signals using SigmaPlot. The time constants (τ) and the FRET ratio signal amplitudes (c) were determined from the fitted curves. F is the FRET ratio signal at time t, F_0 is the baseline FRET ratio signal, c is the FRET ratio signal amplitude of $F - F_0$, c_1 and c_2 are the fluorescence amplitudes of individual exponential components of a double-exponential function and τ is the time constant of the individual exponential component.

2.11. Calcium measurements

Astrocyte-loaded coverslips were incubated for 30 min at room temperature in culture medium supplemented with 5 μM Fluo-4 AM, a cell-permeant fluorescent calcium indicator (Thermo Fisher Scientific, Waltham, MA, USA). Then cells were washed with extracellular solution, incubated for a further 30 min to allow de-esterification of acetoxymethyl ester and mounted into the chamber on a confocal microscope equipped with a Plan-Apochromat air objective 20×/NA 0.8. Fluo-4 was excited by a 488-nm argon laser line and emission fluorescence was filtered with a 495–565 bandpass filter. Time-lapse images were acquired every second for 5 min before and 10 min after the bolus addition of the stimulus, which reached a final concentration of: 0.5 mM 3Cl-5-OH-BA (Santa Cruz Biotechnology, Dallas, TX, USA), 10 mM L-lactate and 100 μM ATP. Time-dependent changes in Fluo-4 fluorescence indicating increases in $[Ca^{2+}]_i$ were acquired by LSM780 software (Zeiss) within manually outlined ROIs that encompassed individual cells. The baseline fluorescence (F_0) was determined at the beginning of each recording as the average intensity (in arbitrary units) during the first 300 frames. Custom-written Matlab software (MathWorks, Natick, MA, USA) was used to obtain the peak calcium amplitude ($\Delta F/F_0$) and the surface under the curve (corresponding to time-integrated calcium amplitudes ($\Delta F/F_0 \times t$)).

2.12. Generation of GLAST::CreERT2/$Gdi1^{flox}$ mice

Heterozygote $Gdi1^{lox/X}$ female mice [8] were crossed with transgenic GLAST::CreERT2 male mice [23] (obtained from M. Götz, Munich, Germany). Mice genotype was analysed by PCR analysis of DNA extracted from the tail using primers Lox1 (5′ GGA AGA CTT GGA AGC TGA AAG CTT T 3′) and Lox2 (5′ CAT GAT GCC AGA CAG GAT GCA TTC 3′), GLAST F8 (5′ GAG GCA CTT GGC TAG GCT CTG AGG A 3′), GLAST R3 (5′ GAG GAG ATC CTG ACC GAT CAG TTG G 3′) and GLAST CER1 (5′ GGT GTA CGG TCA GTA AAT TGG ACA T 3′) as previously described[8; 23]. All animals were maintained on a 12 h light/dark cycle at 22–25 °C. Food pellets and water were available ad libitum.

2.13. Tamoxifen administration

Tamoxifen (Tx, 20 mg/mL solution) (Sigma, St. Louis, Missouri, USA, T-5648) was dissolved in corn oil (Sigma, St. Louis, Missouri, USA, C-8267) at 45 °C for 4 h. To optimize Cre activity induction in the adult brain and obtain $GlastGdi1^{flox/Y}$, thirty days old $GlastGdi1^{lox/Y}$ and WT animals were injected with 100 mg/kg Tx intraperitoneally twice a day for 5 days. NT $GlastGdi1^{lox/Y}$ and WT mice were injected with corn oil. Tx-treated mice were analysed 1 month after the last Tx injection.

2.14. Electron microscopy

Three-month-old $GlastGdi1^{flox/Y}$ and WT littermate mice were perfused transcardially with 2% paraformaldehyde, 2.5% glutaraldehyde, 2 mM $CaCl_2$ in 150 mM cacodylate buffer (pH 7.4). After perfusion, brains were removed from the skull and further fixed over night at 4 °C. A McIlwain tissue chopper was used to obtain 200-mm-thick sagittal slices, and small pieces of the CA1 region were cut with a razor blade. Samples were then post-fixed according to the ROTO procedure (reduced osmium-thiocarbohydrazide-osmium) by sequentially incubating in 1% osmium tetroxide, 1.5% potassium ferrocyanide in 150 mM cacodylate buffer (pH 7.4) for 1 h on ice, 1% thiocarbohydrazide solution in dH_2O for 20 min and 2% osmium tetroxide in dH_2O for 30 min. After rinsing in dH_2O, samples were stained en bloc with uranyl acetate overnight and dehydrated in increasing concentrations of ethanol and propylene oxide, and finally embedded in Epon. Samples were cured at 60 °C in an oven for 48 h. Epon blocks were sectioned using a Leica EM UC7 ultramicrotome (Leica Microsystems, Wetzlar, Germany). Hippocampal CA1 samples were cut from the slide at Bregma – 2.20 mm and – 2.40 mm rostrocaudally. Serial ultrathin sections (60 μm) were collected on pioloform-coated single-slot copper grids and examined with a CM100 electron microscope (Philips Electron Optics, Eindhoven, the Netherlands) at 80 kV.

The selected section was oriented at 700× magnification to select 4 random fields at least 80 μm distant within the middle portion of CA1 stratum radiatum. Four to eight non-overlapping images at 3–5 μm distance were captured per random field at an initial 27,500× magnification. In total, 25 images or an area of 380 μm^2 were sampled for each animal with a Bioscan Camera 792 (Gatan, Pleasanton, CA, USA) using Digital Micrograph 2.5 software (NCMI, Houston, TX, USA). A synapse was identified by the clustering of synaptic vesicles (SVs) and by the presence of a postsynaptic density. Synaptic profiles touching the exclusion lines were not counted. The lengths of active zones, the number of SVs and the areas of the axonal terminals were measured by using ImageJ software. The density of SVs per axon terminal area was obtained by dividing the number of SVs by the cross-section area of the

axonal terminals; the area occupied by mitochondria was subtracted from the total area of axonal terminals.

2.15. Behavioural tests

Animals were maintained on an inverted 12 h light/dark cycle at 22–24 °C. All behavioural procedures were approved by the Animal Care of the San Raffaele Scientific Institute, and by the National Ministry of Health (IACUC nos. 652 and 653). All the behavioural tests were assessed on 3- to 4-month-old mice, comparing *GlastGdi1*$^{flox/Y}$ and *GlastGdi1*$^{X/Y}$ littermates. We used *GlastGdi1*$^{X/Y}$ mice as controls to evaluate the toxicity of the Tx injection and the Cre activity without loxP sites.

2.15.1. Novelty test

Frames of non-reflective aluminium (37-cm high) were used to partition the open field into 4 square 50 × 50 cm arenas, allowing for concurrent observation of 4 animals. The novel object was a 50-mL Falcon tube positioned vertically in the centre of the arena. Each animal was observed for 30 min in the empty arena after 30 min pre-exposure the day before. The novel object was then introduced and observation continued for another 30 min. For the time-course analysis, the total observation time was portioned into 6 periods of 10 min.

2.15.2. Water maze

The standard hidden-platform version of the water maze was done as previously described [24,25]. Briefly, the test included an acquisition phase (18 trials, 6/day, inter-trial time 30–40 min) followed by a reversal phase during which the platform was moved to the opposite position (12 trials, 6/day). The trials were averaged in blocks of 2 trials for the analysis.

2.15.3. Radial maze

The apparatus consisted of 8 arms (38-cm long, 7-cm wide) extending from an octagonal centre platform (diameter 18.5 cm) with 5-cm transparent plastic walls. The distance from the platform centre to the end of each arm was 47 cm. A cup with a food pellet was present at the end of each arm. Food-deprived mice (maintained at 85% of their free-feeding weight) were placed in the centre platform and allowed to collect pellets placed at the end of each arm for 10 min. The animals were adapted to the maze for 1 day and then tested for 10 days. For each trial, the total number of arm choices, the number of correct choices before the first error, and the total number of errors were recorded.

2.15.4. Spontaneous alternation

The apparatus was the same as described for the radial maze with only 4 arms open. A mouse was released in the central hub of a cross maze (4 arms) and left free to explore for 10 min. The number and sequence of arm entries were recorded. A correct alternation was considered when no more than one repetition over 5 entries was made.

2.15.5. Fear conditioning

Contextual and trace fear-conditioning protocols were used. All mice were pre-exposed to the test chamber (Ugo Basile, Gemonio, Italy) for 10 min on the 2 days preceding conditioning. During the training phase of contextual fear conditioning, the trial started with 60 s at baseline followed by presentation of the tone (CS, 15 s) superimposed with the shock (US) in the last 2 s. During the training phase of the trace fear conditioning, the trial started with 60 s at baseline followed by presentation of the tone (CS, 15 s), followed 15 s later by the presentation of the shock US for 2 s. In both protocols, the CS-US presentation was repeated 5 times with a 60-s inter-trial intervals. Twenty-four hours after training conditioning, CTX and CS memory (CUE) were tested. CTX took place in the same chamber and consisted of 2 min observation. CUE memory took place in a different chamber and consisted of 1 min without (Bl, baseline) and 1 min with the CS (CUE).

2.15.6. Spontaneous alternation and fear-conditioning test after 2-deoxy-D-glucose injection

Gdi1 WT and KO mice received an intraperitoneal injection of 10 μL/g 2-DG (Sigma-Aldrich, D-6134) solution 30 min before the 1-day spontaneous alternation test or fear-conditioning test as described above. Treated mice were compared with mice injected with saline solution.

2.16. Video tracking and data collection

Animals were video-tracked using the EthoVision 2.3 system (Noldus Information Technology, Wageningen, the Netherlands; http://www.noldus.com) using an image frequency of 4.2/s. Raw data were transferred to Wintrack 2.4 (http://www.dpwolfer.ch/wintrack) for offline analysis.

For fear-conditioning protocols, animals were video-tracked using the ANY-maze system (Anymaze, Stoelting, Wood Dale, IL, USA; www.anymaze.com).

2.17. In vitro electrophysiology

All procedures were approved by the Italian Ministry of Health and the San Raffaele Scientific Institute Animal Care and Use Committee in accordance with the relevant guidelines and regulations. Mice (30 days of age) were anaesthetized with an intraperitoneal injection of a mixture of ketamine/xylazine (100 mg/kg and 10 mg/kg, respectively) and perfused transcardially with ice-cold artificial cerebrospinal fluid (ACSF) containing 125 mM NaCl, 3.5 mM KCl, 1.25 mM NaH_2PO_4, 2 mM $CaCl_2$, 25 mM $NaHCO_3$, 1 mM $MgCl_2$, and 11 mM D-glucose, saturated with 95% O_2 and 5% CO_2 (pH 7.3). After decapitation, brains were removed from the skull and 300-μm-thick horizontal slices containing the somatosensory cortex were cut in ACSF at 4 °C using a VT1000S vibratome (Leica Microsystems). Individual slices were then submerged in a recording chamber mounted on the stage of an upright BX51WI microscope (Olympus, Tokyo, Japan) equipped with differential interference contrast optics. Slices were perfused with ACSF containing 10 μM gabazine (Abcam, Cambridge, UK) to block $GABA_A$ receptors. The ACSF was continuously flowing at a rate of 2–3 mL/min at 32 °C. Whole-cell patch-clamp recordings were performed in cortical pyramidal cells using pipettes filled with a solution containing 10 mM NaCl, 124 mM KH_2PO_4, 10 mM HEPES, 0.5 mM EGTA, 2 mM $MgCl_2$, 2 mM Na_2-ATP, 0.02 mM Na-GTP (pH 7.2, adjusted with KOH; tip resistance: 4–6 MΩ). During recordings, 2-DG was added to the ACSF at a final concentration of 20 mg/mL and the slice was superfused for 6–8 min before testing its effect on spontaneous EPSCs. For each cell, AMPA-receptor mediated sEPSCs were recorded in a voltage clamp at a holding potential of −70 mV for 1 min. All recordings were performed using a MultiClamp 700B amplifier interfaced with a computer through a Digidata 1440A digitizer (Molecular Devices, Sunnyvale, CA, USA). The liquid junction potential was not corrected. The series resistance was partially compensated (40%–50%) using the amplifier control circuit. Traces were sampled at a frequency of 10 kHz and low-pass filtered at 2 kHz. For each trace, median values of all parameters under study were calculated and analysed. Data were acquired using pClamp10 software (Molecular Devices) and analysed with Clampfit and GraphPad Prism (GraphPad, La Jolla, CA, USA).

2.18. Statistical tests

Unless stated otherwise, the statistics are presented as means ± SEM. Significance levels were $^{***}p < 0.001$, $^{**}p < 0.01$ and $^{*}p < 0.05$; tests are indicated with each experiment. For FRET measurements, unless stated otherwise, Student's *t*-test was performed. In behavioural studies, statistical analyses were done using Statview 5.0 (SAS Institute, Cary, NC, USA); for electrophysiological data statistical comparisons were obtained using SigmaStat 3.5 (Systat, San Jose, CA, USA).

3. Results

3.1. Abnormal astrocytic glucose metabolism in Gdi1 KO mice

How glial-expressed αGDI improves the health of neurons is presently unknown, but it is expected to have an impact on metabolic activity in astrocytes. To evaluate putative changes in protein expression caused by the lack of *Gdi1*, a quantitative proteomic analysis [26] was carried out on *Gdi1* KO and *Gdi1* wild-type (WT) astrocytes, resulting in the identification of 245 proteins to be up- or downregulated in *Gdi1* KO mice compared with WT mice (Supplementary Table 1). Among these proteins, enzymes involved in glucose metabolism were significantly altered in *Gdi1* KO astrocytes: the astrocyte-specific enzyme glycogen phosphorylase, which converts glycogen into glucose-1-phosphate [27], was significantly reduced in *Gdi1* KO astrocytes compared with WT ($p = 0.0001$); an opposite trend occurred with the mitochondrial form of phosphoenolpyruvate carboxykinase (PEPCK 2, $p = 0.025$), which catalyses the generation of glucose from non-carbohydrate carbon substrates such as pyruvate, lactate, glycerol and glucogenic amino acids involved in gluconeogenesis [28,29]. These data suggest an increased demand for glucose availability by increasing astrocytic glucose metabolism in *Gdi1* KO mice.

Because glucose metabolism is essential for normal brain function, including memory formation, we analysed whether glucose handling in *Gdi1* KO brain differs from that in *Gdi1* WT animals. Imaging of ^{18}F-fluorodeoxyglucose ([^{18}F]-FDG), an analogue of D-glucose (2-deoxy-2-[^{18}F]fluoro-D-glucose) which is transformed to [^{18}F]-FDG-6-phosphate by hexokinase and no further metabolized [30], revealed an increased [^{18}F]-FDG radioactivity uptake signal in whole 3-months-old *Gdi1* KO brains compared with WT ($p = 0.05$, Fig. 1a, b). In particular, the strongly enhanced autoradiographic signal in *Gdi1* KO murine brain slices was specific for cortex ($p = 0.02$), hippocampus ($p = 0.04$) and cerebellum ($p = 0.03$) brain regions, but not for the striatum and thalamus (Fig. 1c). These results indicate a specific role of αGDI in D-glucose utilization circumscribed to defined brain areas.

To verify the direct involvement of αGDI in altered D-glucose homeostasis, we first evaluated glucose tolerance and insulin sensitivity, fasting and non-fasting glucose levels. Then, brain astrocytes, an important site of aerobic glycolysis in the brain [31], were studied using the glial fibrillary acidic protein (GFAP) marker to quantify the total astrocytic cell density and analysing the density of the most abundant D-glucose transporter GLUT1. No differences in systemic glucose metabolic readouts were detected between 3-month-old *Gdi1* WT and KO mice (Supplementary Fig. 1a–c). Similarly, by immunofluorescence on *Gdi1* WT and KO cortical brain slices, no alterations between genotypes were detected on GFAP-immunolabelled cells per nm^2, as well as GLUT1-positive cells per nm^2 (Supplementary Fig. 1d). Moreover, the analysis of GLUT1 surface expression by biotinylation assay on *Gdi1* WT and KO astrocytic cell cultures showed no alterations between genotypes (Supplementary Fig. 1e, f). However, these results suggest that the glucose–related metabolic readouts and the canonical glucose-related brain structures appear unaffected by the lack of *Gdi1*, therefore we further tested whether the regulation of astroglial aerobic glycolysis was altered in the two genotypes.

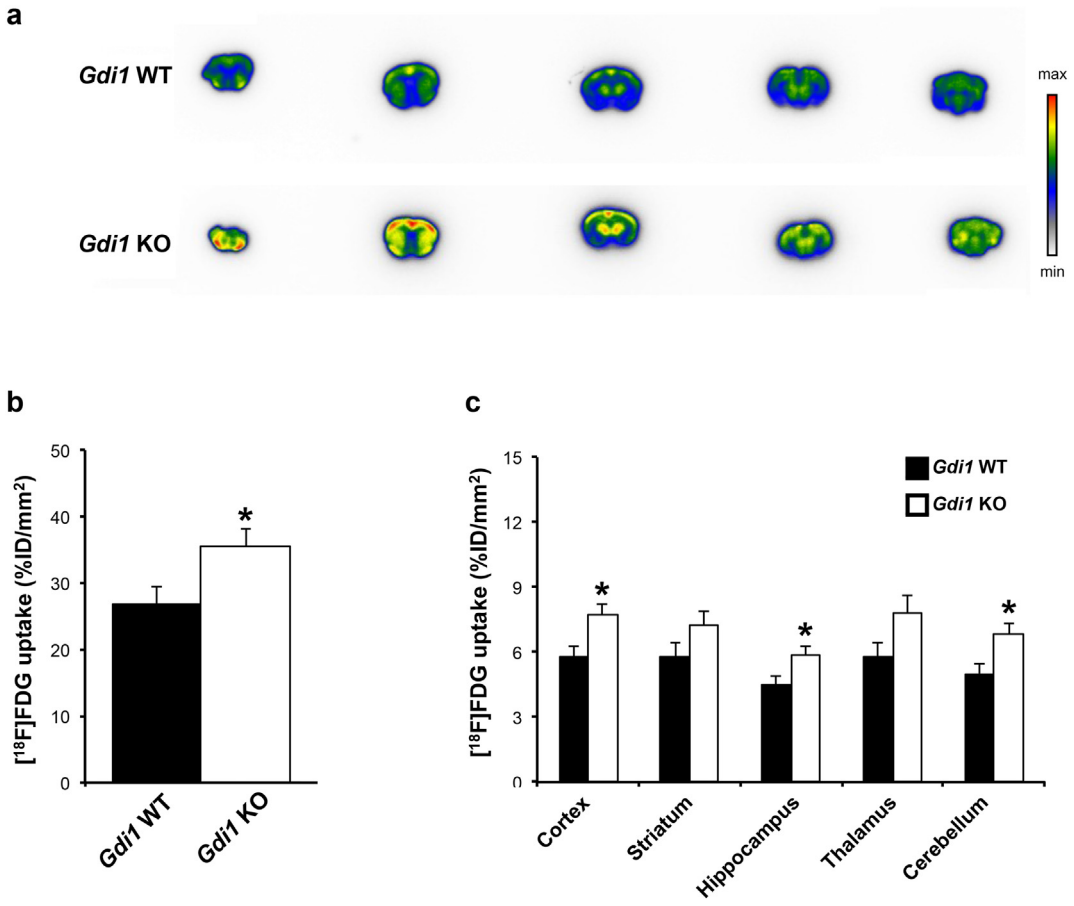

Fig. 1. [^{18}F]-FDG autoradiography of *Gdi1* WT and *Gdi1* KO mouse brains. a Representative [^{18}F]-FDG autoradiography images of coronal brain sections (antero-posterior orientation from left to right) obtained from *Gdi1* WT (top) and *Gdi1* KO (bottom) mice. b Total [^{18}F]-FDG-uptake of the brain areas of *Gdi1* WT (n = 6) and *Gdi1* KO mice (n = 9) obtained in autoradiography studies. The sum of regional [^{18}F]-FDG uptake measured in *Gdi1* KO animals was significantly higher compared with that measured in *Gdi1* WT animals. c [^{18}F]-FDG uptake in discrete brain areas of *Gdi1* WT (n = 6) and *Gdi1* KO mice (n = 9). Black and white bars represent [^{18}F]-FDG uptake in the brain areas of *Gdi1* WT and *Gdi1* KO mice, respectively. [^{18}F]-FDG uptake was calculated as a percentage of the injected dose per area of brain analysed (%ID/mm^2) and expressed as mean ± SEM. Student's *t*-test $^*p < 0.05$.

3.2. Noradrenaline-induced D-glucose utilization associates with extracellular L-lactate modulation of cAMP signalling in Gdi1 KO astrocytes

We assessed whether the increased D-glucose utilization in *Gdi1* KO murine brain (Fig. 1) was associated with changes in the regulation of aerobic glycolysis in astrocytes. For this, we measured cytosolic levels of free D-glucose ($[glucose]_i$), a parameter determined by D-glucose uptake from the extracellular space, and the rate of cellular D-glucose consumption. An increase in $[glucose]_i$ can be recorded in astrocytes under noradrenaline (NA) stimulation, due to facilitated extracellular D-glucose uptake [32], requiring sequestration in the endoplasmic reticulum [33] and stimulated glycogenolysis [20]. We used the fluorescence resonance energy transfer (FRET)-based nanosensor FLII12PGLU-700μΔ6 [20] to monitor $[glucose]_i$ in *Gdi1* KO and *Gdi1* WT astrocytes. The results revealed that in *Gdi1* KO astrocytes, the amplitude of the NA-mediated increase in $[glucose]_i$ was reduced by ~2-fold compared with *Gdi1* WT astrocytes; from 27.1% ± 4.1% (mean ± standard error of the mean [SEM], 14 responsive cells [35%] of 42 cells) to 16.6% ± 2.6% in *Gdi1* KO astrocytes (20 responsive cells [47%] of 42 cells; one-way ANOVA, $p < 0.05$; Fig. 2a, left graph, and b, curve fitting parameters in Supplementary Table 2). However, the time constant (τ), a measure of the kinetics of the NA-mediated increase in $[glucose]_i$, was similar in *Gdi1* WT and KO astrocytes (Fig. 2a, left graph, and b). As these responses were measured at the same extracellular D-glucose concentration, these results are consistent with the view that D-glucose utilization is facilitated in *Gdi1* KO compared with *Gdi1* WT astrocytes.

Facilitated D-glucose utilization is expected to result in accelerated production of L-lactate, which can then exit astrocytes through monocarboxylate transporters (MCTs [34]) and further enhance astroglial glycolysis through a receptor-like mechanism [35]. Indeed, in the presence of 2 mM extracellular L-lactate, a physiological value in the brain [36], NA elicited a reduced amplitude in $[glucose]_i$ in *Gdi1* WT astrocytes (11.4% ± 2.2%; 10 responsive (50%) of 20 cells; Fig. 2a, right graph, and b), significantly lower in comparison with responses in the absence of extracellular L-lactate (Fig. 2a, left graph, 27.1% ± 4.1%), and consistent with facilitated D-glucose utilization in *Gdi1* KO astrocytes. In the presence of 2 mM L-lactate, the amplitude of the NA-induced increase in $[glucose]_i$ in *Gdi1* WT responsive cells was similar to that recorded in *Gdi1* KO astrocytes in the absence of 2 mM L-lactate (Fig. 2a, left graph, and b). Moreover, in the presence of 2 mM extracellular L-lactate, the kinetics (τ) of NA-induced responses in *Gdi1* WT cells was significantly reduced; from 253.5 ± 39.5 s (mean ± SEM; n = 12) in the

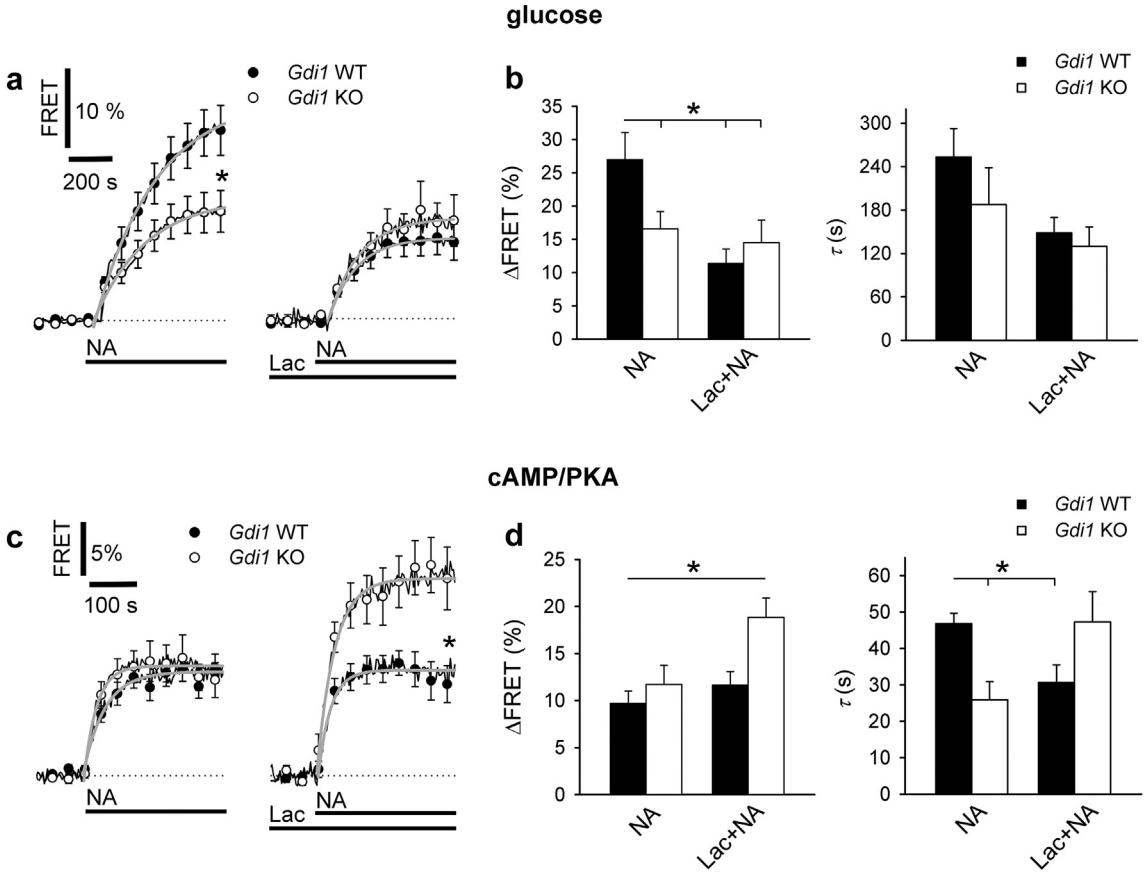

Fig. 2. Noradrenaline-induced increase in cytosolic D-glucose is reduced in astrocytes from *Gdi1* KO versus WT animals. a Mean time-dependent changes in cytosolic D-glucose concentration ($[glucose]_i$), presented as changes in EYFP/ECFP fluorescence (FRET) signal in astrocytes expressing FLII12PGLU-700 μΔ6 on noradrenaline stimulation (NA, 200 μM). Experiments were performed in control (left) and in 2 mM L-lactate pre-treated (Lac) astrocytes (right), isolated from *Gdi1* WT (black; 14 responsive out of 42 cells for NA, 10 responsive out of 20 cells for Lac + NA) and *Gdi1* KO animals (white; 20 responsive out of 42 cells for NA, 8 responsive out of 12 cells for Lac + NA), each obtained on 3 independent cultures. Changes in the FRET signal are expressed as percentages relative to the initial values. Single exponential functions were fitted to the curves (see Supplementary Table 2 for equation parameters). b Mean amplitudes (ΔFRET) and time constants (τ) of NA-induced increase in $[glucose]_i$ from *Gdi1* WT and *Gdi1* KO astrocytes in the absence and presence of 2 mM L-Lactate (NA and Lac + NA, respectively) determined by fitting exponential functions (see parameters in Supplementary Table2). c Mean time-dependent changes in cytosolic cAMP-dependent PKA activity presented as changes in YFP/CFP fluorescence (FRET) signal in astrocytes expressing cAMP/PKA nanosensor AKAR2 on NA stimulation (100 μM). Experiments were performed in control (left) and in 2 mM L-lactate pre-treated (Lac) astrocytes (right) isolated from *Gdi1* WT (black; 12 responsive out of 12 cells [control], 11 responsive out of 11 cells [Lac]) and *Gdi1* KO animals (white; 11 responsive out of 11 cells [control], 12 responsive out of 12 cells [Lac]). Cell cultures were prepared from 5 *Gdi1* WT and 4 *Gdi1* KO animals for NA stimulation; and 4 *Gdi1* WT and 5 *Gdi1* KO animals for NA stimulation on 2 mM L-lactate pre-treated astrocytes. Single exponential functions were fitted to the curves (see Supplementary Table 2 for equation format). d Mean amplitudes (ΔFRET) and time constants (τ) of NA-induced increase in cAMP/PKA activity in *Gdi1* WT and *Gdi1* KO astrocytes in the absence and presence of pre-treatment with 2 mM L-lactate (NA and Lac + NA, respectively) determined by fitting exponentials; parameters in Supplementary Table 2. Error bars in graphs and bar charts denote the mean ± SEM; asterisks in bar charts indicate significant differences (one way ANOVA, $^*p < 0.05$).

absence of 2 mM L-lactate to 148.5 ± 21.3 s (n = 10; one-way ANOVA, $p < 0.05$; Fig. 2b) in the presence of 2 mM L-lactate. However, it was similar to the τ value recorded in *Gdi1* KO astrocytes in the presence of 2 mM extracellular L-lactate: 129.7 ± 27.1 s (mean ± SEM, n = 8 responsive cells (67%) of 12 cells; Fig. 2b, Lac + NA). These data indicate that changes in the physiological levels of extracellular L-lactate, an extracellular signal [37], might facilitate D-glucose utilization in *Gdi1* WT astrocytes to the same extent as in *Gdi1* KO in the absence of added extracellular L-lactate, suggesting that the facilitated utilization of D-glucose in *Gdi1* KO cells was due to changed regulation of aerobic glycolysis.

Because cytoplasmic cAMP/PKA signalling, mediated by β-adrenergic receptors, is involved in the regulation of glycolysis [38], we next used the FRET-based nanosensor AKAR2 to monitor cytosolic cAMP-dependent PKA (cAMP/PKA) activity [39]. The amplitude of cAMP-dependent PKA activity, stimulated by the addition of NA, was similar in both types of astrocytes (Fig. 2c), despite the increased abundance of β_1-adrenergic receptors in *Gdi1* KO compared with WT cells (Supplementary Fig. 2a, b). However, the time constant τ of the increase in PKA activity was significantly shorter in *Gdi1* KO astrocytes than in *Gdi1* WT cells (mean ± SEM in seconds; *Gdi1* WT, 46.8 ± 3.0 s, n = 12 responsive cells (100%); *Gdi1* KO, 26.0 ± 5.0 s, n = 11 responsive cells (100%); one-way ANOVA, $p < 0.05$; Fig. 2d, right graph). Moreover, in the presence of 2 mM extracellular L-lactate (Lac + NA), the cAMP signalling was potentiated by almost 2-fold, however only in *Gdi1* KO astrocytes, where the amplitude relative to the baseline (in %) was significantly larger than the response recorded in the absence of extracellular L-lactate (mean ± SEM in %; *Gdi1* KO, 18.9% ± 2.0%, n = 12 responsive cells (100%); *Gdi1* WT, 11.7% ± 2.0%, n = 11 responsive cells (100%); Student's *t*-test; $p < 0.05$; Fig. 2c, right graph, and d). These results indicate that cAMP signalling was altered in *Gdi1* KO cells and that these cells were more sensitive to changes in extracellular L-lactate (Fig. 2a, c), a putative signal regulating glycolysis in astrocytes [35].

Thus, the extracellular L-lactate-mediated potentiation of NA-induced cAMP signalling in *Gdi1* KO astrocytes (Fig. 2c, d) was likely due to enhanced cAMP production, not only via adrenergic receptors but also L-lactate receptors [35,37,40], because in the absence of NA, the addition of extracellular L-lactate (2 mM) on its own produced a small but significant increase in cAMP signalling in *Gdi1* KO but not in *Gdi1* WT controls (Supplementary Fig. 3).

In addition to cAMP, changes in the cytosolic levels in Ca^{2+} also regulate glycolysis [38] and may contribute to the increased D-glucose utilization in *Gdi1* KO astrocytes observed in these experiments. However, this is unlikely, because addition of extracellular L-lactate (10 mM) had no effect on cytosolic levels of Ca^{2+} in *Gdi1* WT and in *Gdi1* KO astrocytes, as monitored by calcium fluorescence indicator Fluo-4 AM (Supplementary Fig. 4a–c). Collectively, these results indicate that the NA-dependent increase in D-glucose utilization in the presence of extracellular L-lactate in *Gdi1* KO astrocytes is associated with facilitated cAMP, but not with Ca^{2+} signalling.

3.3. Intact capacity of Gdi1 KO astrocytes to produce and transport L-lactate through MCTs

We next asked whether the cAMP signalling involving the putative L-lactate receptor mechanisms [41] is affected in *Gdi1* WT and *Gdi1* KO astrocytes. For this, extracellular L-lactate (20 mM; Fig. 3a) or 3-chloro-5-hydroxybenzoicacid (3-Cl-5-OH-BA, 0.5 mM; Fig. 3b), a selective GPR81 L-lactate receptor agonist [42], were used while monitoring the cAMP-dependent PKA activity. In *Gdi1* WT and KO astrocytes exposed to 20 mM L-lactate, a similar increase in cAMP-dependent PKA activity was recorded (Fig. 3a). Interestingly, in *Gdi1* KO but not in *Gdi1* WT astrocytes, the exposure to extracellular 2 mM L-lactate increased cAMP signalling (Supplementary Fig. 3a). These results indicate that putative L-lactate receptor(s)-mediated cAMP signalling is not affected at 20 mM (Supplementary Fig. 3b), but only at 2 mM extracellular L-lactate (Supplementary Fig. 3a) in *Gdi1* KO cells.

However, when $[glucose]_i$ was monitored, the application of 20 mM extracellular L-lactate elicited a similar amplitude between genotypes (Fig. 3c), but with a 2-fold slower increase in *Gdi1* KO (mean ± SEM in seconds; *Gdi1* WT, 92.9 ± 23.8 s, n = 11; *Gdi1* KO, 184.2 ± 32.6 s, n = 15; Student's *t*-test, $p < 0.05$; Fig. 3c). These data are consistent with the view that D-glucose utilization is facilitated in *Gdi1* KO astrocytes, as observed when cells were stimulated by NA (Fig. 2a).

L-Lactate is an end product of glycolysis and may be released from astrocytes, which can in turn stimulate astrocytes to produce more L-lactate through astroglial surface L-lactate receptors, or L-lactate may enter the cells through lactate transporters/channels and interfere with glycolysis [35]. Measurements of cytosolic levels of L-lactate ($[lactate]_i$) by the FRET-based nanosensor Laconic [22] revealed that by exposing the cells to L-lactate (20 mM), there was no difference in the time course or in the amplitude of $[lactate]_i$ (Fig. 3d). This indicates that the transport of L-lactate through membrane transporters/channels into astrocytes and/or L-lactate receptor-mediated increase in intracellular L-lactate production was not significantly affected in *Gdi1* KO astrocytes. We next addressed whether monocarboxylate L-lactate transporters, MCT1 and MCT4, were impaired in *Gdi1* KO astrocytes by immunofluorescence on *Gdi1* KO and *Gdi1* WT astrocytes. The percentage of MCT1 and MCT4 protein expression in astrocytes was unaltered (Fig. 3e).

Next, to evaluate whether the resting rate of L-lactate production was altered in *Gdi1* KO compared with *Gdi1* WT astrocytes, we monitored $[lactate]_i$ increases in the presence of α-cyano-4-hydroxycinnamate (CHC, 6 mM), a blocker of membrane MCTs. In the absence of L-lactate exchange through the plasma membrane, the predominant pathway available for increase in $[lactate]_i$ is considered to be glycolytic L-lactate production [35]. Although cytosolic L-lactate levels may be coupled to mitochondrial metabolism in astrocytes [43,44], in the presence of MCT blockers, the increase in $[lactate]_i$ is comparable with the rate of aerobic glycolysis at rest. After the application of CHC, we observed an exponential increase in $[lactate]_i$. Fitting an exponential curve revealed that the amplitude (c) and the kinetics (expressed by the time constant τ) were similar in *Gdi1* WT and KO astrocytes (Supplementary Table 4).

Together, these results indicate that in *Gdi1* KO astrocytes, facilitated D-glucose utilization persists, with no impact on the capacity of these cells to produce and transport L-lactate through MCT transporters.

3.4. Generation of an astrocyte-inducible Gdi1 conditional null mouse

To test how altered astroglial D-glucose metabolism contributes to the previously reported *Gdi1* KO cognitive dysfunctions [7], we generated an inducible *Gdi1* KO mouse carrying the *Gdi1* deletion only in adult astrocytes, and we tested for its behavioural performance. To inactivate *Gdi1* prevalently in astrocytes, the previously generated heterozygous $Gdi1^{lox/X}$ female mice [8] were crossed with transgenic *GLAST::CreERT*^{2} male mice (obtained from M. Götz, Munich, Germany), a tamoxifen-inducible form of Cre-recombinase under the astrocyte-specific glutamate transporter (GLAST) promoter, known to allow gene deletion in adult astrocytes at a precise time [23]. The breeding generated *GLAST::CreERT*$^{2+}$/$Gdi1^{lox/Y}$ male mice (referred to as *GlastGdi1*$^{flox/Y}$ for astrocyte-specific *Gdi1* KO), which were compared with the $Gdi1^{X/Y}$ WT male littermate mice. *Gdi1* tamoxifen-inducible astrocytic inactivation was assessed in 150-day-old (P) *GlastGdi1*$^{flox/Y}$ and WT cortical brain slices. Tamoxifen toxicity was excluded because of the comparable GFAP-positive astrocyte density between genotypes (Fig. 4a, b). In situ hybridization and immunofluorescence were coupled to reveal the distribution of *Gdi1* mRNA in GFAP-positive astrocytes (Fig. 4a, b). Comparing the number of *Gdi1* and GFAP double-positive cells in *GlastGdi1*$^{flox/Y}$ and $Gdi1^{X/Y}$ mice, we found that 58% of astrocytes showed *Gdi1* inactivation (mean ± SEM as the

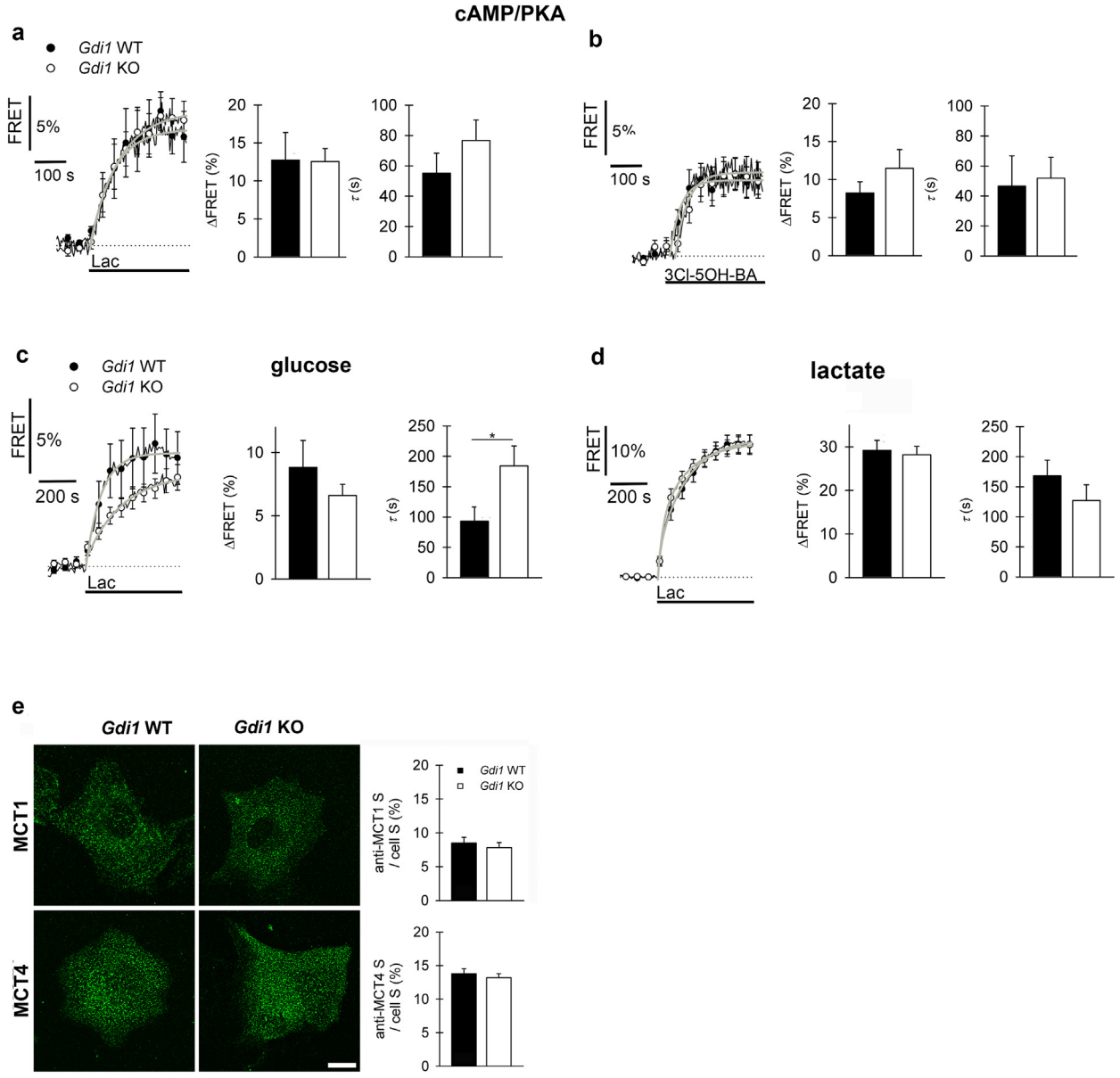

Fig. 3. Reduced rate of $[glucose]_i$ increase upon extracellular L-lactate stimulation in *Gdi1* KO astrocytes. a–b Mean time-dependent changes in cytosolic cAMP/PKA activity (YFP/CFP fluorescence (FRET) signal; AKAR2 nanosensor) elicited (a) by 20 mM L-lactate (Lac) and (b) by 0.5 mM GPR81 L-lactate receptor agonist 3-chloro-5-hidroxybenzoat (3Cl-5-OH-BA) in *Gdi1* WT astrocytes (black; 7 responsive out of 13 cells for Lac, 5 responsive out of 8 cells for 3Cl-5-OH-BA) and *Gdi1* KO cells (white; 9 responsive out of 17 cells for Lac, 11 responsive out of 12 cells for 3Cl-5-OH-BA); cultures were obtained from 4 *Gdi1* WT and 5 KO animals for 20 mM Lac and from 2 *Gdi1* WT and 2 KO animals for 3Cl-5-OH-BA. Exponential functions were fitted to the curves (Supplementary Table 3); parameters are in histograms to the right in (a) and (b). The onset of FRET response upon 3Cl-5-OH-BA stimulation was 28.0 ± 13.0 s in *Gdi1* WT, shorter than 43.6 ± 7.2 s in *Gdi1* KO astrocytes. c-d Mean time-dependent changes in (c) $[glucose]_i$ (EYFP/ECFP fluorescence (FRET) signal; FLII12PGLU-700 μΔ6 nanosensor) in *Gdi1* WT (black; 11 responsive out of 12 cells) and *Gdi1* KO astrocytes (white; 15 responsive out of 22 cells) and (d) $[lactate]_i$ (mTFP/Venus fluorescence (FRET) signal; Laconic nanosensor) in *Gdi1* WT (black; 24 responsive out of 25 cells) and *Gdi1* KO astrocytes (white; 22 responsive out of 24 cells), elicited by 20 mM extracellular L-lactate (Lac); cells were from at least 3 independent *Gdi1* WT and KO cultures. Parameters of fitted exponentials (Supplementary Table 3) are in histograms to the right. The amplitude of $[glucose]_i$ increase was similar in *Gdi1* WT and KO astrocytes, whereas time constant was >2-fold larger in *Gdi1* KO versus *Gdi1* WT astrocytes. Changes in the FRET signal in (a–d) are expressed as percentages relative to the initial values. e Representative images of *Gdi1* WT and KO astrocytes labelled with antibodies against MCT1 or MCT4. Scale bar, 20 μm. Bar charts of relative anti-MCT1-, anti-MCT4-positive cell cross-section area (S; i.e. number of green fluorescence pixels, threshold >20% of maximal fluorescence) versus total cell cross-section area (cell S; i.e. number of all pixels) in percent (%) in *Gdi1* WT and KO astrocytes; MCT1 experiment, 3 and 4 *Gdi1* WT and *Gdi1* KO independent cultures, respectively; MCT4 experiments, 6 and 7 *Gdi1* WT and KO independent cultures, respectively. Error bars are means ± SEM, Mann-Whitney *U* test, $^*p < 0.05$.

number of *Gdi1* and GFAP double-stained cells/nm^2; $Gdi1^{X/Y}$, 0.80 ± 0.18; $GlastGdi1^{flox/Y}$, 0.34 ± 0.05; n = 3 mice per genotype; Student's *t*-test, $p = 0.01$; Fig. 4a, b), in agreement with the Cre-recombinase efficiency described previously [23].

The experiments also demonstrated that the lack of *Gdi1* is specifically limited to the astrocytes, without neuronal involvement, because by electron microscopy in the CA1 hippocampal terminals, we found no alterations in synaptic button morphology and synaptic vesicle density (Table 1), as has been shown to be the major morphological phenotype observed in *Gdi1* KO mice [45].

3.5. $GlastGdi1^{flox/Y}$ mice are specifically impaired in working memory but not in associative memory

It was previously shown that adult *Gdi1* KO mice as well as neuronal-specific $CaMKII\text{-}Cre^{+}\text{-}Gdi1^{flox/Y}$ mice did not have defects in emotional or

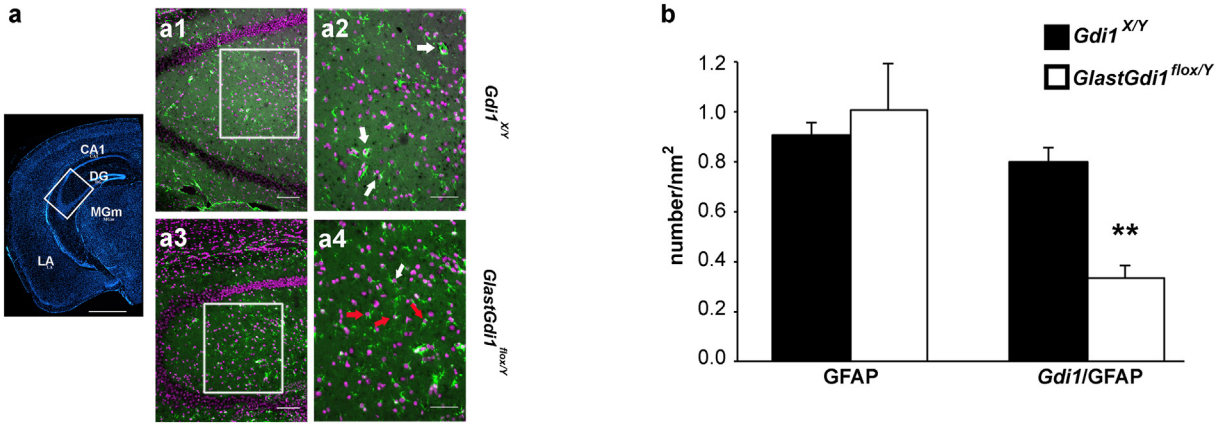

Fig. 4. Characterization of *GlastGdi1*$^{flox/Y}$ mice. a Left panel is a low magnification coronal section stained with DAPI. The white rectangle outlines the hippocampal region analysed in (a_1)–(a_4). Scale bar, 1 mm. DG, dentate gyrus; CA1, hippocampal CA1 region; LA, lateral amygdala; MGm, medial geniculate nucleus. a_1–a_4 Representative images of *Gdi1* in situ hybridization (black), GFAP immunofluorescence (green) and DAPI (purple). (a_1) correspond to *Gdi1*$^{X/Y}$ and (a_2) is a magnification outlined by the white square in (a_1); the same for *GlastGdi1*$^{flox/Y}$ (a_3 and a_4). White arrows indicate GFAP-positive cells co-localizing with *Gdi1*; red arrows indicate GFAP-positive cells that are negative for *Gdi1*. Scale bars, 100 μm (a_1 and a_3); 50 μm (a_2 and a_4). b Histograms represent the mean ± S.E.M of the GFAP-positive cells and the colocalization between GFAP and *Gdi1*-positive cells/nm^2 of the CA1 region of stratum radiatum of the hippocampus from *Gdi1*$^{X/Y}$ (n = 3; black) and *GlastGdi1*$^{flox/Y}$ (n = 3; white) mice. Student's *t*-test, $^{**}p < 0.01$.

Table 1
Electron microscopy quantification of pre-synaptic parameters in the CA1 hippocampal region of *GLASTGdi1*$^{lox/Y}$ versus *GlastGdi1*$^{flox/Y}$ mice.

	GLASTGdi1$^{lox/Y}$	*GlastGdi1*$^{flox/Y}$
No. of mice analysed	3	3
No. of synapses analysed	243	261
Synapsis density (no./μm^2)	0.40 ± 0.01	0.40 ± 0.01
Pre-synaptic area (μm^2)	0.23 ± 0.01	0.24 ± 0.01
PSD length (μm)	0.30 ± 0.01	0.30 ± 0.01
SV density (no. SV/μm^2)	106 ± 3.55	107 ± 3.44

Statistical analysis was performed using the unpaired Student's *t*-test *GLASTGdi1*$^{lox/Y}$ versus *GlastGdi1*$^{flox/Y}$. PSD, postsynaptic density; SV, synaptic vesicle.

exploratory behaviour but were selectively impaired in anterior forebrain-dependent forms of short-term memory, the working and associative fear-related memory, the radial maze and trace fear-conditioning tests [7,8,45], respectively. To assess whether astrocytic αGDI ablation in postnatal life plays a key role in working and associative fear-related memory formation, P90 *Gdi1*$^{X/Y}$ and *GlastGdi1*$^{flox/Y}$ male littermate mice were subjected to the following tests: novelty test to assess explorative behaviour, water maze test to evaluate spatial memory, 8-arm radial maze to analyse working and procedural memory, and fear conditioning to estimate associative memory. To exclude any toxic effects due to Cre-recombinase expression and/or tamoxifen injection, we used WT male mice for *Gdi1* (*Gdi1*$^{X/Y}$) but carrying the *GLAST:CreERT*^{2} transgene (*GlastGdi1*$^{X/Y}$) treated with tamoxifen and tested at P90. *GlastGdi1*$^{X/Y}$ mice were indistinguishable from the *Gdi1*$^{X/Y}$ mice in all the tests (data not shown).

Then, we first assessed exploratory behaviour and spatial memory in *Gdi1*$^{X/Y}$ and *GlastGdi1*$^{flox/Y}$ male littermates by the novelty test and water maze, respectively. Both groups showed normal explorative behaviour, as shown for the distance travelled (Fig. 5a), as well as intact spatial memory scored by the time to reach the hidden platform in the water maze task (Fig. 5b) or in the probe trial (Fig. 5c). Because similar performances were also observed in *Gdi1* KO mice as well as neuronal-specific *CaMKIIGdi1*$^{flox/Y}$ mice, we concluded that the lack of αGDI in neurons or astrocytes did not affect exploration and spatial memory.

Next, we assessed spatial working memory by subjecting the animals to the 8-arm radial maze and the spontaneous alternation test. As shown in Fig. 5d, in the 8-arm radial maze, the total number of errors declined over the 10 days of training in both *Gdi1*$^{X/Y}$ and *GlastGdi1*$^{flox/Y}$; however, acquisition in mutant mice was significantly slower than in controls (ANOVA repeated measures for genotype effect $F[1,51] = 6.6$, $p = 0.01$), and they did not reach the performance level of *Gdi1*$^{X/Y}$ mice. Although *Gdi1*$^{X/Y}$ mice eventually reached nearly perfect performance (7 out of a maximum number of 8 correct successive arm visits; Fig. 5e), *GlastGdi1*$^{flox/Y}$ mice barely scored above chance level (5.5 correct successive arm visits after 10 days of training; ANOVA repeated measures for genotype effect $F[1,51] = 6.5$, $p = 0.01$; Fig. 5e). Accordingly, in the spontaneous alternation test, a significant difference was observed between genotypes in the percentage (%) of correct alternation (ANOVA factorial analysis for genotype effect $F[1,13] = 9.1$, $p = 0.01$; Fig. 5f). Thus, the lack of αGDI in astrocytes affects spatial working memory.

One of the most robust phenotypes that we always observed in the *Gdi1* KO mice was the specific inability to associate stimuli across a short time interval, as we showed in the trace fear-conditioning paradigm (TFc) but not in the standard protocol (termed delay or contextual conditioning, DFc) [7]. We then subjected the animals to both paradigms and surprisingly, *GlastGdi1*$^{flox/Y}$ mice showed intact associative learning in both tests (Fig. 5g–l). No difference was observed between *Gdi1*$^{X/Y}$ and *GlastGdi1*$^{flox/Y}$ mice in any of the tests performed: the ability to associate a tone, a conditioned stimulus (CS), with a foot shock, an unconditioned stimulus (US), during the training session (Fig. 5g, j); as well as 24 h later when tested for context memory (Fig. 5h, k) and the cue memory test (Fig. 5i, l).

These results revealed that *GlastGdi1*$^{flox/Y}$ mice exhibit selective impairment of working memory ability, demonstrating that although

Fig. 5. Behavioural analysis of *GlastGdi1*$^{flox/Y}$ mice. a Distance travelled during the novelty test by *GlastGdi1*$^{flox/Y}$ (n = 10) and *Gdi1*$^{X/Y}$ (n = 8) mice. b, c Water Maze test. b Time to reach the hidden platform by *GlastGdi1*$^{flox/Y}$ (n = 10) and *Gdi1*$^{X/Y}$ (n = 7) mice during 5 consecutive days. c Annulus crossing during the probe trial in the first 30 s of the first day of the reversal phase. oo, opposite old goal position; ol, left side of old goal position; og, old goal; or, right side of old goal. d, e Radial maze test. d Number of errors done by *GlastGdi1*$^{flox/Y}$ (n = 27) and *Gdi1*$^{X/Y}$ (n = 26) mice in the 10 consecutive days. e Number of correct arm choices before the first error. f Percentage (%) of correct alternations during the spontaneous alternation test done by *GlastGdi1*$^{flox/Y}$ (n = 9) and *Gdi1*$^{X/Y}$ (n = 6) mice. g–i Contextual (delay) fear-conditioning test assessed in *GlastGdi1*$^{flox/Y}$ (n = 12) and *Gdi1*$^{X/Y}$ (n = 13) animals. g Percentage (%) of freezing displayed during the 15 s of the 5 CS presentations in the training session, (h) during the context memory test and (i) during the CUE test. j–l Trace fear conditioning assessed in *GlastGdi1*$^{flox/Y}$ (n = 19) and *Gdi1*$^{X/Y}$ (n = 15) animals. j Percentage (%) of freezing displayed during the 15 s of the 5 CS presentations in the training session, (k) during the context memory test and (i) during the CUE test. Data points and histograms represent the means ± SEM. Black bars and circles represent *Gdi1*$^{X/Y}$ and white bars and circles represent *GlastGdi1*$^{flox/Y}$. ANOVA, $^{*}p < 0.05$.

associative fear-related memory was dependent on αGDI function in neurons, working memory ability relied on αGDI-independent function(s) in neurons and astrocytes (Table 2). Moreover, we could speculate that alteration in working memory ability could be triggered by facilitated D-glucose utilization in *Gdi1* KO mice (Fig. 1), as demonstrated in isolated astrocytes (Figs. 2 and 3).

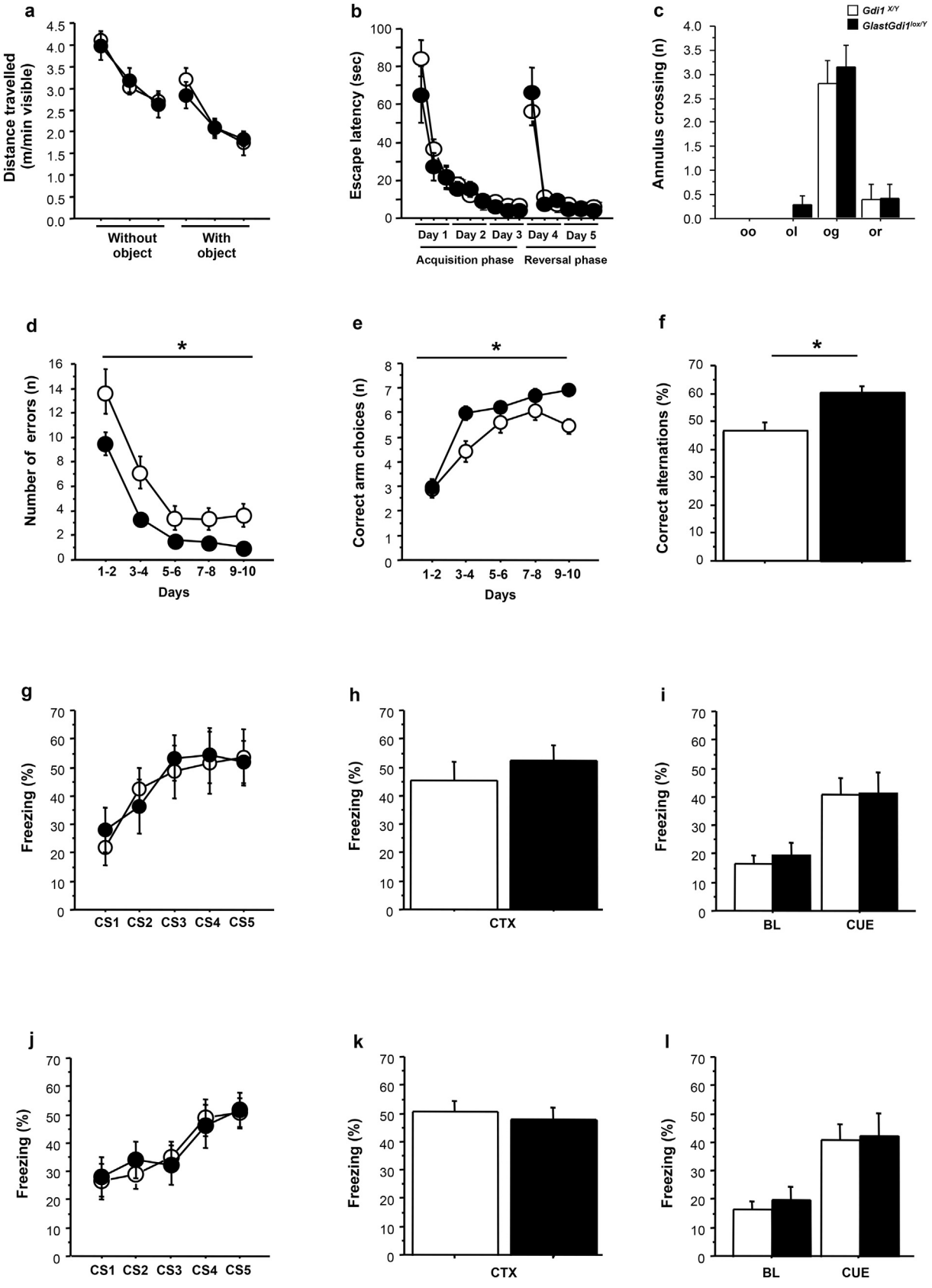

Table 2
Comparison between *Gdi1* mouse models in behavioural studies.

Tests	*Gdi1* KO (full)	*CamKIIGdi1*$^{flox/Y}$ (neuronal)	*GLASTGdi1*$^{flox/Y}$ (astroglial)
Novelty	☑	☑	☑
Water maze	☑	☑	☑
8-Arm radial maze and spontaneous alternation	↓	↓	↓
Contextual fear conditioning	☑	☑	☑
Trace fear conditioning	↓	↓	☑

☑, no differences between genotypes; ↓, impairment in learning, compared to Gdi1 WT.

3.6. Acute 2-deoxy-D-glucose treatment ameliorates working memory performance in Gdi1 KO mice

We then tested whether impaired glucose metabolism, demonstrated by the more efficient use of D-glucose in *Gdi1* KO astrocytes (Figs. 2a, 3b), consistent with an enhanced [^{18}F]-FDG signal (Fig. 1), was the key process underlying the working memory defect in *Gdi1* KO mice, as also shown to be specific in *GlastGdi1*$^{flox/Y}$ mice (Fig. 5d–f). The replacement of 3 mM D-glucose in the extracellular solution with 0 mM D-glucose or 3 mM 2-deoxy-D-glucose (2-DG), which enters cells through glucose transporters and blocks glycolysis [12], greatly reduced the NA-induced increase in $[lactate]_i$ in rat cortical astrocytes (Supplementary Table 5). We then treated *Gdi1* KO and WT littermate mice with 2-DG and compared them with non-treated (NT) groups in the spontaneous alternation working memory test and the trace fear-conditioning associative test as a negative control. We also treated *Gdi1* KO and WT mouse littermates with 3Cl-5-OH-BA, a GPR81 receptor agonist [42], which increases L-lactate production in astrocytes [35].

As shown in Fig. 6a, injection of 2-DG significantly impaired the score for the spontaneous alteration test of *Gdi1* WT animals compared with NT *Gdi1* WT mice (ANOVA factorial analysis for 2-DG versus NT effect on WTs: $F[1,42] = 28.3$, $p < 0.0001$). In contrast, the 2-DG treatment significantly improved the performance of *Gdi1* KO mice compared with NT *Gdi1* KO mice (ANOVA factorial analysis for treatment effect on KO: $F[1,41] = 9.6$, $p = 0.003$); in particular, *Gdi1* KO 2-DG-treated mice reached the performance level of NT *Gdi1* WT mice. The injection of 3Cl-5-OH-BA had no effect on *Gdi1* KO mice and worsened the score for the spontaneous alteration test of treated *Gdi1* WT compared with NT *Gdi1* WT (ANOVA factorial analysis for 3Cl-5-OH-BA-WT versus NT-WT effect: $F[1,37] = 17.08$, $p = 0.0002$; Fig. 6a).

Conversely, the treatment of *Gdi1* KO and WT mouse littermates with 2-DG compared with NT groups in the trace fear-conditioning test had no significant effect on *Gdi1* WT mice in any of the test sessions. Instead, injection of 2-DG in *Gdi1* KO mice improved their performance slightly during the training and context sessions but not during the tone test compared with NT *Gdi1* KO mice (ANOVA repeated measures for 2-DG KO versus NT-KO training effect for CSs: $F[1,23] = 5.8$, $p = 0.02$; context memory [CTX] effect: $F[1,23] = 4.8$, $p = 0.03$; Fig. 6b–d).

These results strongly support the view that facilitated utilization of D-glucose in astroglial aerobic glycolysis has a negative impact on working memory acquisition, but not on trace fear conditioning, as shown by the performance of *Gdi1* WT mice under 2-DG treatment.

We then investigated how 2-DG treatment affects cortical glutamatergic transmission, by recording spontaneous excitatory postsynaptic currents (sEPSCs) in cortical slices from 2-DG-treated and NT P30 *Gdi1* KO and WT littermate mice using whole-cell voltage-clamp recordings (Fig. 6e–h). Compared with WT, *Gdi1* KO neurons showed decreased average frequency and increased average amplitude of sEPSCs (mean ± SEM for frequency in Hz; *Gdi1* WT, 6.6 ± 0.7 Hz, n = 10; *Gdi1* KO, 4.8 ± 0.5 Hz, n = 11 cells; unpaired Student's *t*-test, $p = 0.03$; Fig. 6f; mean ± SEM for amplitude in pA; *Gdi1* WT, −7.5 ± 0.9 pA, n = 12; *Gdi1* KO, −10.6 ± 1.1 pA, n = 10 cells; unpaired Student's t-test, $p = 0.04$; Fig. 6g), without showing any changes in the decay time constant (Fig. 6h). Extracellular perfusion with 2-DG caused a significant increase in the average sEPSC frequency in *Gdi1* KO but not in WT neurons (mean ± SEM for frequency in Hz; NT-KO, 5.1 ± 0.6 Hz; 2-DG-KO, 7.4 ± 0.6 Hz, n = 11; paired Student's t-test, $p = 0.013$; Fig. 6f). Conversely, the peak amplitude and decay time constant were unaffected by 2-DG in both genotypes (Fig. 6g, h). These results indicate that presynaptic glutamate release is reduced in *Gdi1* KO neurons in comparison with *Gdi1* WT and is rescued after acute treatment with 2-DG.

4. Discussion

In this study, we describe a new phenotype associated with *Gdi1* deletion in mouse brain related to alterations in astrocytic glucose metabolism. ^{18}[F]-FDG imaging in *Gdi1* KO mouse brain revealed increased glucose uptake in specific regions. In addition, proteomic experiments on *Gdi1* KO astrocytes have shown that enzymes involved in the mobilization/production of glucose are modulated differently in *Gdi1* KO mice, suggestive of increased D-glucose utilization. This was confirmed by single astrocyte FRET experiments measuring cAMP/PKA activity, cytosolic levels of D-glucose ($[glucose]_i$) and L-lactate ($[lactate]_i$), which revealed that D-glucose utilization was facilitated in *Gdi1* KO astrocytes compared with *Gdi1* WT astrocytes.

L-Lactate is an important product of astrocytic aerobic glycolysis, which cannot be easily produced in neurons, but represents a fuel for neuronal oxidative metabolism [46]. Interestingly, the capacity of L-lactate export from *Gdi1* WT and KO astrocytes was similar, determined by unchanged expression of MCT1 and MCT4 monocarboxylic acid transporters by immunocytochemistry. This was confirmed functionally by monitoring $[lactate]_i$ while exposing astrocytes to 20 mM extracellular L-lactate, although the rate of L-lactate-induced increase in $[glucose]_i$ was >2-fold slower in *Gdi1* KO versus WT astrocytes.

The increased sensitivity of cAMP signalling in *Gdi1* KO astrocytes to extracellular L-lactate (2 mM) likely arises from an altered set and/or density of receptors in *Gdi1* KO versus WT astrocytes. These membrane

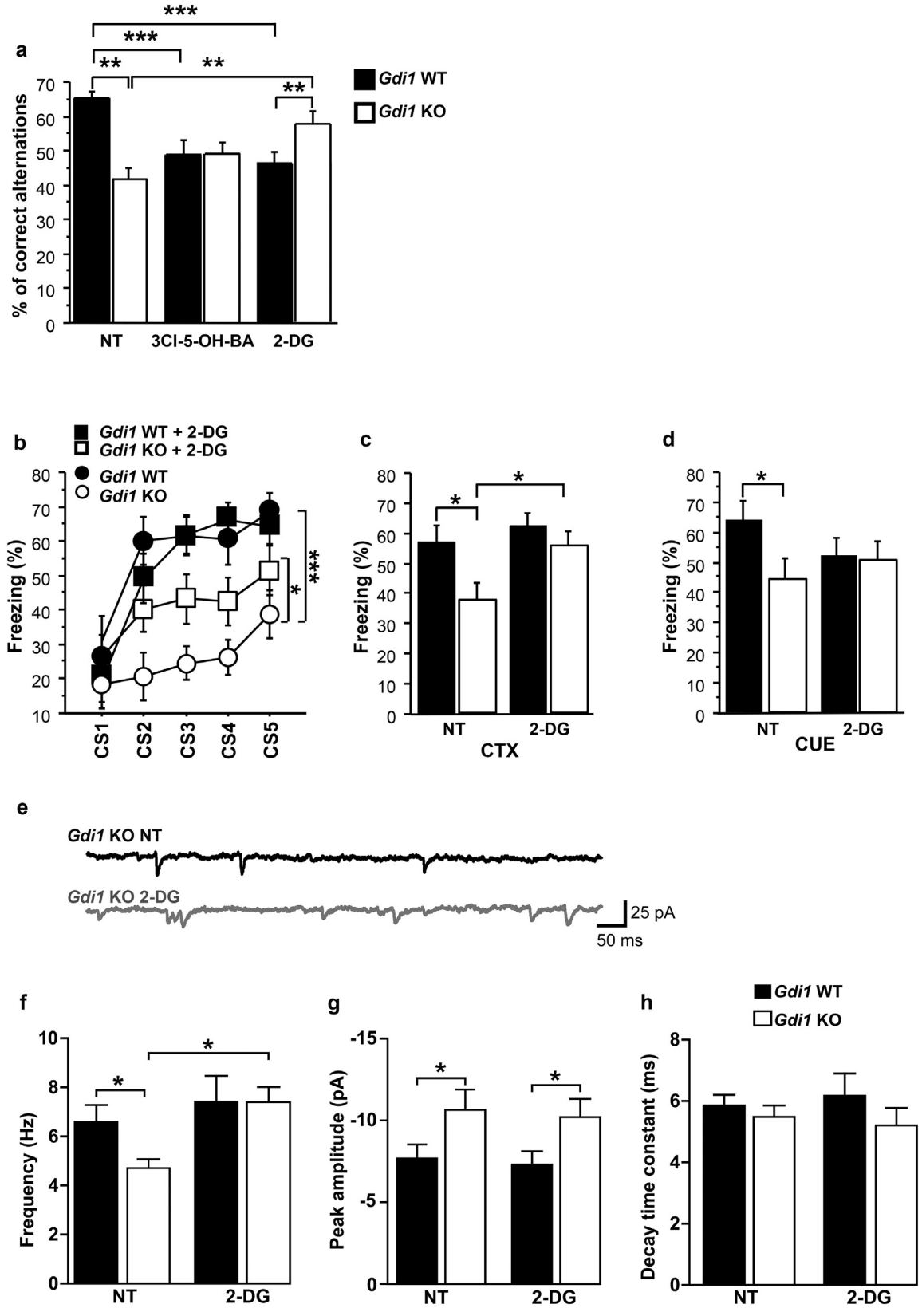

Fig. 6. 2-Deoxy-D-glucose treatment improves cognition in *Gdi1* KO mice. a Percentage (%) of correct alternations of 2-deoxy-D-glucose (2-DG)-treated WT (n = 18) and *Gdi1* KO (n = 13) mice, 3-chloro-5-hidroxybenzoic acid (3Cl-5-OH-BA)-treated WT (n = 13) and *Gdi1* KO (n = 12) mice compared with non-treated (NT) WT (n = 26) and *Gdi1* KO (n = 30) mice. Data are expressed as means ± SEM. b–d Percentage (%) of freezing during the training (b), context (c) and cue (tone) (d) trace fear-conditioning test of 2-DG-treated WT (n = 13) and *Gdi1* KO (n = 12) mice compared with non-treated (NT) WT (n = 16) and *Gdi1* KO (n = 13) mice. e Representative traces showing sEPSCs recorded in pyramidal neurons of slices from *Gdi1* KO mice in NT conditions (black trace) and after bath perfusion with 2-DG (grey trace). f–h Summary data for EPSC parameters obtained from WT and KO cortical neurons. Data are expressed as means ± SEM. ANOVA was used for behavioural test; Student's t-test was used for electrophysiological parameters; $^{*}p < 0.05$, $^{**}p < 0.01$, $^{***}p < 0.001$.

receptors are delivered to the plasma membrane by vesicles; thus, in part, the mechanism for an altered array of surface membrane receptors, as determined by monitoring the abundance of adrenergic receptors, is likely linked to the general change in vesicle dynamics described in *Gdi1* KO astrocytes previously [47]. In addition to defective vesicle network dynamics, the more sensitive L-lactate-mediated increase in cAMP in *Gdi1* KO astrocytes might also be due to putative oligomerization between different G-protein coupled (GPCR) receptor types [35,48]. Moreover, this can also be due to the overexpression of L-lactate-sensitive receptors.

The identity of L-lactate receptors in the brain has been considered in primary cortical neurons, where extracellular L-lactate modulates neuronal activity via a receptor-mediated process [49], recently described as the HCAR 1 (GPR81) receptor [50], the canonical L-lactate receptor, originally discovered in adipocytes [51]. However, this receptor is unlikely present in the locus coeruleus neuronal somata [40], where a multitude of L-lactate receptors may play a role [41].

The nature of L-lactate receptors in astrocytes is also unknown, but unlikely involves GPR81, which has been shown to reduce the levels of cAMP in adipocytes through an autocrine loop [51]. In astrocytes, the application of selective agonists for GPR81 resulted in an increase in cAMP, even in the absence of GPR81, indicating novel, yet unidentified L-lactate receptors in these cells [35]. The results in this study are consistent with these findings, both at the cell level and at the level of behaviour, where application of the GPR81 agonist 3Cl-5-OH-BA increased cAMP activity (Fig. 3b), a stimulus for aerobic glycolysis in astrocytes [31], and tended to worsen the behavioural phenotype of correct alteration (Fig. 6a), respectively.

The overall aim of our study was to test the hypothesis that previously observed cognitive impairment of *Gdi1* KO animals arises not only from a deficit in synaptic glutamate release of excitatory neurons but also from a metabolic defect in astrocytes. This was confirmed by generating an inducible *Gdi1* deletion selectively in astrocytes, which revealed a particular role of astrocytic αGDI in anterior forebrain-related working memory acquisition. Many studies have been performed to establish the astrocytic role in animal behaviour, independently addressing the neuron-astrocyte network (for a review see Oliveira et al. [9]). Our results strongly support the view that the significantly increased [^{18}F]-FDG radioactivity uptake in hippocampus and cortical brain regions and the facilitated utilization of D-glucose in astrocytes, through aerobic glycolysis, has a negative impact on working memory acquisition in the neurodevelopmental disease, represented by the *Gdi1* KO animals. To further test this hypothesis, *Gdi1* KO and WT animals were treated with 2-DG. This treatment was able to reverse the working memory defect in *Gdi1* KO mice by competing with high D-glucose entry but also associative memory, probably acting on neuronal activity. Moreover, the results that working, but not associative short-term, memory formation was affected by astrocytic αGDI ablation in postnatal life is consistent with the view that astrocytes act as signal integrators due to their very slow stimulus-vesicle secretion coupling [52,53].

The electrophysiological data indicate that the frequency of spontaneous glutamatergic ESPCs in cortical neurons was reduced in *Gdi1* KO mice as compared to WT, suggesting a decrease in presynaptic glutamate release. Such effect is consistent with the cognitive deficits we observed in *Gdi1* KO mice (Fig. 5). We also detected an increase in the average sEPSC amplitude in *Gdi1* KO mice, perhaps due to a compensatory effect against reduced frequency. Since αGDI is involved in controlling vesicle trafficking, we cannot exclude a direct negative impact on vesicle release in slices from *Gdi1* KO mice. However, 2-DG significantly restored the diminished frequency of sEPSC in *Gdi1* KO mice, confirming that this deficit is caused, at least in part, by facilitated glycolysis and D-glucose utilization. Interestingly, extracellular perfusion with 2-DG exerted no significant effects on sEPSCs in WT slices, consistent with a recent report [54]. Moreover, increased D-glucose utilization may result in excessive local L-lactate availability for synapses. Recent data reported that lactate attenuates glutamatergic synaptic transmission and perturbs network oscillations in gamma and theta-gamma frequency ranges in hippocampal slices [55], again supporting the view that synaptic and cognitive deficits in our model are caused by metabolic dysfunctions.

In summary, the results in this study revealed that in the *Gdi1* mouse XLID model, the utilization of D-glucose by astrocytes is facilitated. The nature of this change arises from the mutation of *Gdi1* causing a pleiotropic deregulation primarily of vesicle traffic [47], and secondarily altering the cell surface signalling landscape regulating aerobic glycolysis in astrocytes. This was demonstrated by slightly increased adrenergic receptors at the plasma membrane and by the increased sensitivity of cAMP signalling to relatively low levels of extracellular L-lactate, which activates a yet unknown L-lactate receptor. Moreover, based on immunocytochemistry of MCT1 and MCT4 and measurements of the intracellular concentration of L-lactate, the transport of L-lactate across the plasma membrane appears unchanged. However, the NA- and 3Cl-5-OH-BA-induced increase in $[glucose]_i$ appears changed, indicating a more efficient utilization of D-glucose in aerobic glycolysis in *Gdi1* KO astrocytes. In support of this, administration of 2-DG, which can enter cells, but cannot be metabolized to generate L-lactate, reverses working memory impairment in *Gdi1* KO mice. Thus, astrocyte-based glycolytic mechanisms may represent a novel target strategy to treat intellectual disability. Moreover, our data are consistent with a previous report showing that metabolic reprogramming in astrocytes is present in a Huntington mice model [56], however, whether the changes in D-glucose utilization observed in our study affect also mitochondrial metabolism, needs to be further studied.

Supplementary data to this article can be found online at https://doi.org/10.1016/j.metabol.2020.154463.

Funding

The support by grants from the Slovenian Research Agency (P3 310, J3 4051, J3 4146, L3 3654; J3 3236, J36790, J36789, J3 7605), CIPKEBIP (P3-0310, J3-9266), COST Action CA18133 (ERNEST), COST Nanonet, COST Mouse Ageing, COST CM1207 - GLISTEN, and the Comitato Telethon Fondazione ONLUS (TCP04015) and by the Roche Postdoctoral Fellowship program (RPF #138, F. Hoffmann-La Roche AG, Switzerland).

Ethics approval

All animal procedures were conducted in accordance with the International Guiding Principles for Biomedical Research Involving Animals developed by the Council for International Organizations of Medical Sciences and Animal Protection Act (Official Gazette of the Republic of Slovenia, No. 38/13), in accordance with the guidelines established by the European Community Council Directive of 24 November 1986 on the use of animals in research (86/609/EEC). The experimental protocol was approved by The Administration of the Republic of Slovenia for Food Safety, Veterinary and Plant Protection (Republic of Slovenia, Ministry of Agriculture, Forestry and Food, Dunajska cesta 22, 1000 Ljubljana), document no. U34401-47/2014/7 and U34401-48/2014/7. The animal experiments were done according to the animal protocols approved by the Institutional Animal Care and Use Committee San Raffaele (IACUC) (San Raffaele, Milan, Italy) and were approved by the National Ministry of Health, Italy (IACUC ID 652). All efforts were made to minimize animal suffering and to use only the number of animals necessary to produce reliable results.

Availability of data and material

All data generated or analysed during this study are included in this article and its Supplementary Information, Data in Brief, files or are available from the corresponding author on reasonable request.

CRediT authorship contribution statement

P.D. designed, generated and characterized the *GlastGdi1*$^{flox/y}$ mice (molecularly, biochemically and behaviourally), and performed the 2-DG experiments on *Gdi1* KO mice with the help of A.G., M.L.M., V.B., M.M.; S.T. and M.R. performed the electrophysiological experiments; A.B. and U.R. performed proteomic studies; S.B. and R.M.M. performed imaging studies; A.H., J.V.M., M. Malamr, M. Muhič, K.F., M.P., S.T.B., M.K., H.H.C. and M.S. performed experiments and analysed single-cell and proteomics data; A.M. and L.P. performed systemic glucose homeostasis experiments; P.D., N.V. and R.Z. conceived and directed the study and wrote the manuscript. All authors read and contributed to the completion of the draft manuscript.

Declaration of competing interest

The authors declare no competing financial interests.

Acknowledgements

The authors thank Drs W.B. Frommer for providing FLII12PGLU-700 μΔ6, M. Lohse for providing Epac1-camps, R.Y. Tsien for providing AKAR2, L.F. Barros for providing Laconic, and M, Götz for providing the *GLAST::CreERT*^{2} male mice. A. Raimondi at ALEMBIC facility at San Raffaele Scientific Institute, Milan, Italy for the help in electron microscopy experiments and U. Gubenšek, P. Runovc and M. Pate from the Institute of Pathophysiology, Ljubljana, Slovenia for the help with the experiments.

References

[1] Srivastava AK, Schwartz CE. Intellectual disability and autism spectrum disorders: causal genes and molecular mechanisms. Neurosci Biobehav Rev. 2014;46(Pt 2):161–74.
[2] Chiurazzi P, Schwartz CE, Gecz J, Neri G. XLMR genes: update 2007. Eur J Hum Genet. 2008;16(4):422–34.
[3] Lisik MZ, Sieron AL. X-linked mental retardation. Med Sci Monit. 2008;14(11):RA221–9.
[4] Ropers HH. Genetics of intellectual disability. Curr Opin Genet Dev. 2008;18(3):241–50.
[5] Curie A, Sacco S, Bussy G, de Saint Martin A, Boddaert N, Chanraud S, et al. Impairment of cerebello-thalamo-frontal pathway in Rab-GDI mutated patients with pure mental deficiency. Eur J Med Genet. 2009;52(1):6–13.
[6] Stenmark H. Rab GTPases as coordinators of vesicle traffic. Nat Rev Mol Cell Biol. 2009;10(8):513–25.
[7] D'Adamo P, Welzl H, Papadimitriou S, Raffaele di Barletta M, Tiveron C, Tatangelo L, et al. Deletion of the mental retardation gene Gdi1 impairs associative memory and alters social behavior in mice. Hum Mol Genet. 2002;11(21):2567–80.
[8] Bianchi V, Gambino F, Muzio L, Toniolo D, Humeau Y, D'Adamo P. Forebrain deletion of αGDI in adult mice worsens the pre-synaptic deficit at cortico-lateral amygdala synaptic connections. PLoS One. 2012;7(1):e29763.
[9] Oliveira JF, Sardinha VM, Guerra-Gomes S, Araque A, Sousa N. Do stars govern our actions? Astrocyte involvement in rodent behavior. Trends Neurosci. 2015;38(9):535–49.
[10] Verkhratsky A, Parpura V. Astrogliopathology in neurological, neurodevelopmental and psychiatric disorders. Neurobiol Dis. 2016;85:254–61.
[11] Vardjan N, Verkhratsky A, Zorec R. Pathologic potential of astrocytic vesicle traffic: new targets to treat neurologic diseases? Cell Transplant. 2015;24(4):599–612.
[12] Wick AN, Drury DR, Nakada HI, Wolfe JB. Localization of the primary metabolic block produced by 2-deoxyglucose. J Biol Chem. 1957;224(2):963–9.
[13] Schwartz J, Wilson D. Preparation and characterization of type 1 astrocytes cultured from adult rat cortex, cerebellum, and striatum. Glia. 1992;5(1):75–80.
[14] Giannandrea M, Bianchi V, Mignogna ML, Sirri A, Carrabino S, D'Elia E, et al. Mutations in the small GTPase gene RAB39B are responsible for X-linked mental retardation associated with autism, epilepsy, and macrocephaly. Am J Hum Genet. 2010;86(2):185–95.
[15] Shevchenko A, Tomas H, Havlis J, Olsen JV, Mann M. In-gel digestion for mass spectrometric characterization of proteins and proteomes. Nat Protoc. 2006;1(6):2856–60.
[16] Cox J, Mann M. MaxQuant enables high peptide identification rates, individualized p.p.b.-range mass accuracies and proteome-wide protein quantification. Nat Biotechnol. 2008;26(12):1367–72.
[17] Cox J, Neuhauser N, Michalski A, Scheltema RA, Olsen JV, Mann M. Andromeda: a peptide search engine integrated into the MaxQuant environment. J Proteome Res. 2011;10(4):1794–805.
[18] Diering GH, Gustina AS, Huganir RL. PKA-GluA1 coupling via AKAP5 controls AMPA receptor phosphorylation and cell-surface targeting during bidirectional homeostatic plasticity. Neuron. 2014;84(4):790–805.
[19] Zhang J, Hupfeld CJ, Taylor SS, Olefsky JM, Tsien RY. Insulin disrupts beta-adrenergic signalling to protein kinase A in adipocytes. Nature. 2005;437(7058):569–73.
[20] Prebil M, Vardjan N, Jensen J, Zorec R, Kreft M. Dynamic monitoring of cytosolic glucose in single astrocytes. Glia. 2011;59(6):903–13.
[21] Takanaga H, Chaudhuri B, Frommer WB. GLUT1 and GLUT9 as major contributors to glucose influx in HepG2 cells identified by a high sensitivity intramolecular FRET glucose sensor. Biochim Biophys Acta. 2008;1778(4):1091–9.
[22] San Martin A, Ceballo S, Ruminot I, Lerchundi R, Frommer WB, Barros LF. A genetically encoded FRET lactate sensor and its use to detect the Warburg effect in single cancer cells. PLoS One. 2013;8(2):e57712.
[23] Mori T, Tanaka K, Buffo A, Wurst W, Kühn R, Götz M. Inducible gene deletion in astroglia and radial glia—a valuable tool for functional and lineage analysis. Glia. 2006;54(1):21–34.
[24] Lipp HP, Wolfer DP. Genetically modified mice and cognition. Curr Opin Neurobiol. 1998;8(2):272–80.
[25] Wolfer DP, Lipp HP. A new computer program for detailed off-line analysis of swimming navigation in the Morris water maze. J Neurosci Methods. 1992;41(1):65–74.
[26] Ong SE, Blagoev B, Kratchmarova I, Kristensen DB, Steen H, Pandey A, et al. Stable isotope labeling by amino acids in cell culture, SILAC, as a simple and accurate approach to expression proteomics. Mol Cell Proteomics. 2002;1(5):376–86.
[27] Oe Y, Baba O, Ashida H, Nakamura KC, Hirase H. Glycogen distribution in the microwave-fixed mouse brain reveals heterogeneous astrocytic patterns. Glia. 2016;64(9):1532–45.
[28] Schmoll D, Fuhrmann E, Gebhardt R, Hamprecht B. Significant amounts of glycogen are synthesized from 3-carbon compounds in astroglial primary cultures from mice with participation of the mitochondrial phosphoenolpyruvate carboxykinase isoenzyme. Eur J Biochem. 1995;227(1–2):308–15.
[29] Yip J, Geng X, Shen J, Ding Y. Cerebral gluconeogenesis and diseases. Front Pharmacol. 2017;7:521.
[30] Kelloff GJ, Hoffman JM, Johnson B, Scher HI, Siegel BA, Cheng EY, et al. Progress and promise of FDG-PET imaging for cancer patient management and oncologic drug development. Clin Cancer Res. 2005;11(8):2785–808.
[31] Dienel GA. Brain glucose metabolism: integration of energetics with function. Physiol Rev. 2019;99(1):949–1045.
[32] Catus SL, Gibbs ME, Sato M, Summers RJ, Hutchinson DS. Role of β-adrenoceptors in glucose uptake in astrocytes using β-adrenoceptor knockout mice. Br J Pharmacol. 2011;162(8):1700–15.
[33] Muller MS, Fouyssac M, Taylor CW. Effective glucose uptake by human astrocytes requires its sequestration in the endoplasmic reticulum by glucose-6-phosphatase-beta. Curr Biol. 2018;28(21):3481–6 [e3484].
[34] Machler P, Wyss MT, Elsayed M, Stobart J, Gutierrez R, von Faber-Castell A, et al. In vivo evidence for a lactate gradient from astrocytes to neurons. Cell Metab. 2016;23(1):94–102.
[35] Vardjan N, Chowdhury HH, Horvat A, Velebit J, Malnar M, Muhic M, et al. Enhancement of astroglial aerobic glycolysis by extracellular lactate-mediated increase in cAMP. Front Mol Neurosci. 2018:11.
[36] Magistretti PJ, Allaman I. Lactate in the brain: from metabolic end-product to signalling molecule. Nat Rev Neurosci. 2018;19(4):235–49.
[37] Lauritzen KH, Morland C, Puchades M, Holm-Hansen S, Hagelin EM, Lauritzen F, et al. Lactate receptor sites link neurotransmission, neurovascular coupling, and brain energy metabolism. Cereb Cortex. 2014;24(10):2784–95.
[38] Hertz L, Xu J, Peng L. Glycogenolysis and purinergic signaling. Adv Neurobiol. 2014;11:31–54.
[39] Vardjan N, Kreft M, Zorec R. Dynamics of β-adrenergic/cAMP signaling and morphological changes in cultured astrocytes. Glia. 2014;62(4):566–79.
[40] Tang F, Lane S, Korsak A, Paton JF, Gourine AV, Kasparov S, et al. Lactate-mediated glia-neuronal signalling in the mammalian brain. Nat Commun. 2014;5:3284.
[41] Mosienko V, Rasooli-Nejad S, Kishi K, De Both M, Jane D, Huentelman MJ, et al. Putative receptors underpinning l-lactate signalling in locus coeruleus. Neuroglia. 2018;1(2)(2):365–80.
[42] Dvorak CA, Liu C, Shelton J, Kuei C, Sutton SW, Lovenberg TW, et al. Identification of hydroxybenzoic acids as selective lactate receptor (GPR81) agonists with antilipolytic effects. ACS Med Chem Lett. 2012;3(8):637–9.
[43] Passarella S, de Bari L, Valenti D, Pizzuto R, Paventi G, Atlante A. Mitochondria and L-lactate metabolism. FEBS Lett. 2008;582(25–26):3569–76.
[44] Sonnewald U, Westergaard N, Petersen SB, Unsgard G, Schousboe A. Metabolism of [U-13C]glutamate in astrocytes studied by 13C NMR spectroscopy: incorporation of more label into lactate than into glutamine demonstrates the importance of the tricarboxylic acid cycle. J Neurochem. 1993;61(3):1179–82.
[45] Bianchi V, Farisello P, Baldelli P, Meskenaite V, Milanese M, Vecellio M, et al. Cognitive impairment in Gdi1-deficient mice is associated with altered synaptic vesicle pools and short-term synaptic plasticity, and can be corrected by appropriate learning training. Hum Mol Genet. 2009;18(1):105–17.
[46] Barros LF. Metabolic signaling by lactate in the brain. Trends Neurosci. 2013;36(7):396–404.
[47] Potokar M, Jorgačevski J, Lacovich V, Kreft M, Vardjan N, Bianchi V, et al. Impaired αGDI function in the X-linked intellectual disability: the impact on astroglia vesicle dynamics. Mol Neurobiol in press; 2016.
[48] Wacker D, Stevens RC, Roth BL. How ligands illuminate GPCR molecular pharmacology. Cell. 2017;170(3):414–27.

[49] Bozzo L, Puyal J, Chatton JY. Lactate modulates the activity of primary cortical neurons through a receptor-mediated pathway. PLoS One. 2013;8(8):e71721.
[50] de Castro Abrantes H, Briquet M, Schmuziger C, Restivo L, Puyal J, Rosenberg N, et al. The lactate receptor HCAR1 modulates neuronal network activity through the activation of Galpha and Gbetagamma subunits. J Neurosci. 2019;39(23):4422–33.
[51] Ahmed K, Tunaru S, Tang C, Muller M, Gille A, Sassmann A, et al. An autocrine lactate loop mediates insulin-dependent inhibition of lipolysis through GPR81. Cell Metab. 2010;11(4):311–9.
[52] Kreft M, Stenovec M, Rupnik M, Grilc S, Krzan M, Potokar M, et al. Properties of Ca(2+)-dependent exocytosis in cultured astrocytes. Glia. 2004;46(4):437–45.
[53] Zorec R, Horvat A, Vardjan N, Verkhratsky A. Memory formation shaped by astroglia. Front Integr Neurosci. 2015;9:56.
[54] Pan YZ, Sutula TP, Rutecki PA. 2-Deoxy-d-glucose reduces epileptiform activity by presynaptic mechanisms. J Neurophysiol. 2019;121(4):1092–101.
[55] Hollnagel JO, Cesetti T, Schneider J, Vazetdinova A, Valiullina-Rakhmatullina F, Lewen A, et al. Lactate attenuates synaptic transmission and affects brain rhythms featuring high energy expenditure. iScience. 2020;23(7):101316.
[56] Polyzos AA, Lee DY, Datta R, Hauser M, Budworth H, Holt A, et al. Metabolic reprogramming in astrocytes distinguishes region-specific neuronal susceptibility in Huntington mice. Cell Metab. 2019;29(6):1258–73 [e1211].